ADDIS ABABA UNIVERSITY

ADDIS ABABA INSTITUTE OF TECHNOLOGY

SCHOOL OF CIVIL AND ENVIRONMENTAL ENGINEERING

Parametric Analysis of Natural Draft Hyperbolic Cooling Tower under Seismic Load

---

A Thesis in Structural Engineering

By: Tesfa Azage

July, 2019

Addis Ababa

A Thesis

Submitted in Partial Fulfillment of the Requirements for the Degree of Master of Science

The undersigned have examined the thesis entitled '**Parametric Analysis of Natural Draft Hyperbolic Cooling Tower under Seismic Load'** presented by **Tesfa Azage**, a candidate for the degree of **Master of Science** and hereby certify that it is worthy of acceptance.

Dr. Shifferaw Taye		
Advisor	Signature	Date
Dr. Abreham Gebre		
Internal Examiner	Signature	Date
Dr.-Ing. Bedilu Habte		
External Examiner	Signature	Date
Dr. Henok Fikre		
Chair person	Signature	Date

UNDERTAKING

I certify that research work titled "**Parametric Analysis of Natural Draft Hyperbolic Cooling Tower under Seismic Load**" is my own work. The work has not been presented elsewhere for assessment. Where material has been used from other sources it has been properly acknowledged / referred.

Tesfa Azage

ABSTRACT

Hyperbolic cooling towers are large, thin shell reinforced concrete structures which contribute to environmental protection and to power generation efficiency and reliability. They may be subjected to a variety of loading conditions such as self-weight, wind, earthquake, temperature and construction loads, among others.

In this study, the dynamic behavior of hyperbolic cooling towers with various geometric properties under earthquake effect is examined. Geometrical parameter ratios of the cooling tower's dimensions are considered in order to cover a wider spectrum of the cooling tower's geometry. Various cooling tower samples with different geometric dimensions are analyzed and the effects of curvature, slenderness, thickness and throat level on the dynamic behavior of hyperbolic cooling towers are investigated. The influences of these parameters on the behavior of cooling tower are investigated by comparing lateral displacement, hoop force, meridional forces and moments. Numerical analysis are performed using a SAP2000 structural analysis software package.

Finally, the hyperbolic cooling tower lateral displacement, force and moment changes due to the effect of geometric parameters are presented graphically and discussed in detail. The findings can be used as a basis for further research and establishment of conceptual design guidelines when considering seismic load on the dynamic behavior of cooling tower.

Keywords: Hyperbolic cooling tower, Dynamic analysis, Earthquake

.

ACKNOWLEDGMENTS

First, all praises to God Almighty, ever Gracious and Merciful, the ultimate source of knowledge and rationality. Then, I wish to express my sincere thanks and gratitude to my advisor Dr. Shifferaw Taye for his tremendous support including meticulous attention throughout the duration of research.

Finally, a special word of thanks goes out to my parents. They selflessly encouraged me to pursue my aspirations, even though it took me away from their cuddle. Their emphasis on the importance of education helps me to this day, and I cannot thank them enough for all their unwavering support in everything I do.

TABLE OF CONTENTS

ABSTRACT ..... **IV**

ACKNOWLEDGMENTS ..... **V**

TABLE OF CONTENTS ..... **VI**

LIST OF TABLES ..... **VIII**

LIST OF FIGURES ..... **IX**

CHAPTER 1 INTRODUCTION **1**

1.1 Background 1

1.2 Statement of Problem 2

1.3 Objective 2

1.3.1 General Objective 2

1.3.2 Specific Objective 3

1.4 Scope of the Study 3

CHAPTER 2 LITERATURE REVIEW **4**

2.1 Introduction 4

2.2 Dynamic Response – Free Vibrations 5

2.2.1 Theoretical studies 5

2.2.2 Numerical studies 7

2.2.3 Experimental and field studies 9

2.3 Dynamic Response - Forced Vibrations 10

2.3.1 Theoretical Studies 10

2.3.2 Numerical Studies 11

2.3.3 Experimental and Field Studies 13

2.4 Damage to Shell Structures Due to Earthquake 15

2.5 Conclusion of the Literature Review 16

CHAPTER 3 MATERIAL AND METHODS **18**

3.1 Material 18

3.2 Geometry 18

3.3 Parametric Study 22

3.4 Earthquake Loading 25

3.5 Method for Scaling or Matching Ground Motion Records 25
3.5.1 U.S.A. Standard (ASCE/SEI 7-10) 25
3.5.2 ES EN 1998-1:2015 26
3.6 Ground Motion Records and Target Spectrum 27
3.7 Finite Element Modeling 30
3.8 Verification of Software 31
3.9 Dynamic Analysis Method 34
3.9.1 Modal Dynamic Analysis 34
3.9.2 Response Convergence with Mode Numbers 35
CHAPTER 4 ANALYSIS RESULT AND DISCUSSION 36
4.1 Introduction 36
4.2 Horizontal displacement 36
4.3 Hoop, Meridional and Shear Forces along Height 39
4.3.1 Hoop Force 39
4.3.2 Meridional Force 42
4.3.3 Shear Force 44
4.3.4 Moment 46
4.4 Hoop, Meridional and Shear Forces around Circumference (Angular Direction) 48
4.4.1 Hoop, Meridional and Shear Forces at the Base of the Tower 48
4.4.2 Meridional and Shear Forces at the Neck Level of the Tower 54
4.4.3 Meridional Forces at the Peak Level of the Tower 58
CHAPTER 5 CONCLUSION AND RECOMMENDATION 60
5.1 Conclusion 60
5.1.1 Displacement, Force and Moment along Height 60
5.1.2 Force at Base, Neck and Peak Level of the Tower in Angular Direction 61
5.2 Recommendation 61
REFERENCES 62
APPENDIX A 66
APPENDIX B 71

LIST OF TABLES

Table 2.1 Natural frequencies of the clamped-free hyperbolic cooling tower shell (Kim, et al., 2015) 7
Table 2.2 Lowest natural frequencies of column-supported cooling tower (Bhimaraddi, et al., 1991) 8
Table 3.1 Geometric parameter of reference model 21
Table 3.2 Earthquake ground motion records 27
Table 3.3 Finite element model verification; comparison of present results with those previously stablished solutions 31
Table 4.1 Maximum horizontal displacement U1 (cm) 37
Table 4.2 Maximum hoop force 40
Table 4.3 Maximum meridional force at zero degree 42
Table 4.4 Maximum meridional shear force 44
Table 4.5 Maximum meridional moment at zero degree 46
Table 4.6 Maximum shear force at the base 51
Table 4.7 Maximum shear force at the neck 54
Table 4.8 Maximum meridional force at the neck 56
Table 4.9 Maximum meridional force at the peak 58

LIST OF FIGURES

Figure 2.1 Overview of the cooling tower geometry, Shape-finding process: dependence of shell reinforcement on shell thickness (Busch, et al., 2002) 6
Figure 2.2 (a) regions of soil and structure model, (b) Experimental model setup of cooling tower (Shu & Wen-da, 1990) 9
Figure 2.3 (a) Cooling tower shell discretization, (b) Cooling tower structural model (Kopenetz & Catarig, 2011) respectively 11
Figure 2.4 Plastic hinges formed in the finite element model (Sabhouri-Ghomi & Kharrazi, 2005) 14
Figure 2.5 Scaled cooling tower: (a) scaled tower with templates removed; (b) scaled tower with weight blocks added. 15
Figure 3.1 Hyperbolic shell of revolution-geometry (Gould 1977) 18
Figure 3.2 Meridional stress variation along the height of axisymmetric shell structure with change of meridian curvature (Gould, 1977; redrawn Nasir et al., 2000a) 20
Figure 3.3 Hyperbolic cooling tower reference model 22
Figure 3.4 Cooling tower views with varying throat diameter or curvature 23
Figure 3.5 Cooling towers views for various slenderness ratios (appearance) 24
Figure 3.6 Cooling tower views for various throat levels 24
Figure 3.7 Response spectra and time history ground motion actual record 28
Figure 3.8 Matched spectra and time history ground motion 29
Figure 3.9 Comparison of analytic solution and sap2000 software 33
Figure 4.1 Vertical variation of the horizontal displacements 38
Figure 4.2 Location of the local axis set. 39
Figure 4.3 Change of the circumferential (hoop) forces (F11) along the height 41
Figure 4.4 Change of the meridional forces (F22) along the height 43
Figure 4.5 Change of the shear forces (F12) along the height 45
Figure 4.6 Change of the meridional moments along the height 47
Figure 4.7 Angular variation of circumferential (hoop) forces at the base of the tower 49
Figure 4.8 Angular variation of meridional forces at the base of the tower 50
Figure 4.9 Angular variation of shear forces at the base of the tower 52
Figure 4.10 Angular variation of meridional moment at the base of the tower 53
Figure 4.11 Angular variation of circumferential (hoop) forces at neck level 55
Figure 4.12 Angular variation of meridional forces at neck level 57
Figure 4.13 Angular variation of the meridional forces at the peak level 59

CHAPTER 1 INTRODUCTION

1.1 Background

Cooling towers, usually referred to as hyperbolic natural draft towers, are large, thin, reinforced concrete shell structures used for cooling large quantities of water in thermal or atomic power stations and other industrial plants like steel plants and refineries. The cooling operation inside the tower is by airflow through the tower. The rising airflow is produced by the difference in air density that exists between the less dense heated air inside the tower and the denser cooler ambient air outside. Owing to the huge amounts of heated water through the power stations, the height and diameter of the cooling tower are generally huge. It is normal practice to have diameters of cooling towers up to 100m and heights of up to 200m. The thickness of the shell is generally very small compared to the principal radii of curvature of the shell. The cooling tower shell is therefore generally very tall, thin, with a large base diameter, and therefore possesses a huge surface area and a very low mass to surface area ratio.

The cooling tower shell is supported by a truss or framework of columns bridging the air inlet to the tower foundation. They may be subjected to a variety of loading conditions such as self-weight, wind load, earthquake load, temperature and construction loads. The two loading types affect different parts of the structure. When their size is determined, of course, as geography and meteorological conditions are influential the amount of attraction is also important. Sliding they are built piece by piece using mold technique. Own as well as earthquakes and winds, especially dimensions are the most important burdens that determine. While the earthquake activates the entire 360° cross section, the wind load tends to concentrate its influence over only about 180°. This has a marked effect upon the amplification of the loading forces into the meridional shell forces.

Earthquake loads constitute the main loading for the design of cooling towers constructed around the regions prone to severe earthquakes. The loads applied by a design earthquake to the shell and components of a cooling tower can be determined by the response spectrum method which is one of the most appropriate technique requiring a free vibration analysis to evaluate the natural frequencies.

In other words, the magnitude of the earthquake-induced forces is a function of the dynamic properties of the structures such as natural frequency. Therefore, free vibration characteristics of such cooling tower structures are crucial in the design process. Since the vibration response depends on the geometry of the shell wall, supporting columns, raft and soil foundation, considerably these components should be modeled in appropriate detail for a pure earthquake design.

1.2 Statement of Problem

Although hyperbolic natural draft cooling tower shell structures are economically, aesthetically and structurally efficient and reliable for large industrial area, they are not practically available in Ethiopia except the one now the time under construction. Most part of our country is located in the zone of Great Rift Valley so it is prone to the earthquake excitation.

These cooling tower structure is mostly designed to wind load. While the earthquake activates the entire 360° cross section, the wind load tends to concentrate its influence over only about 180°. This has a marked effect upon the amplification of the loading forces into the meridional shell force of the cooling tower that located in seismic region. Besides, their analysis and design were limited to what codes, researchers and manuals postulated in our country. Now a day, the appearance of computer will minimize the tedious hand calculation. In this study, the parametric analysis of natural hyperbolic cooling tower under seismic load analyzed using sap2000 software finite element package. About the earthquake behavior of the cooling towers to any parametric work that will guide the designer are not encountered. For this reason, the dynamic behavior of hyperbolic cooling tower to be maintained by changing geometric parameters.

1.3 Objective

1.3.1 General Objective

The main objective of this study is to analyze the hyperbolic natural draft cooling tower under seismic load by varying its height, neck/throat level and radius with appropriate ratio.

1.3.2 Specific Objective

It is intended to study the effects of curvature, slenderness, thickness and throat level on the dynamic behavior of cooling tower by varying the height, neck/throat level and radius with appropriate ratio.

The influence of these parameter on the behavior of cooling towers will be investigated by comparing lateral displacement, hoop, meridional effect and moments.

Furthermore, this study will try to develop a graph that show the variation of displacement meridional force and moment at any section of the shell.

1.4 Scope of the Study

The hyperbolic natural draft cooling towers are subjected to many different loads such as wind, earthquake, dead, live, construction and temperature load. However, this research paper is discussed to investigate study and analyze the dynamic behavior of cooling tower under seismic load only. And also the parametric analysis is limited to the only geometric dimension and it cannot allow to use bring together all parameter varying the same time but keeping one parameter constant relative to other.

CHAPTER 2 LITERATURE REVIEW

2.1 Introduction

In their paper, (Bamu & Zingoni, 2005) summarized the research developments on concrete hyperbolic cooling tower damage, deterioration and long-term structural performance. A trace of the developments in the research on concrete hyperbolic cooling tower shells with particular attention to the issues of concrete deterioration, durability, long-term performance, condition surveys and strengthening, collapse and the lack of proper collapse documentation was performed. They confirmed research by others for the period from 1961 to 2005.

A comprehensive review of studies done on modelling analysis, design, theoretical and practical investigations on cooling towers between 2005 and 2014 was performed by (Asadzadeh & Alam, 2014). Their survey concluded that a huge amount of research had gone into investigating the geometry and shape optimization of the cooling tower. This development had started as early as in 1967 when the first cooling tower shell was analyzed using the shell bending theory (Krivoshapko, 2002). The Finite Element Method (FEM) had begun to be used as a tool for analysis of the hyperbolic cooling tower shell in the 1970's (Asadzadeh and Alam, 2014). Followed by this was an era of research into numerical solutions of symmetrical from 2005 to 2014 is mostly related to the FEM and analysis of the hyperbolic cooling tower considering material nonlinearity and formation of cracks, large displacements and the use of multilevel elements in the FEM methods.

Asadzadeh and Alam (2014) summarized research done on the response of the hyperbolic cooling tower to earthquake and wind forces. They also summarized research done on the effect of stiffening rings, interference effects of cooling tower groups exposed to wind loading and the soil structure interaction of cooling towers. Their survey tracked the latest theoretical and experimental research improvements in the analysis and design of the natural draft hyperbolic cooling towers.

2.2 Dynamic Response – Free Vibrations

2.2.1 Theoretical studies

(Wen-da & Shi-qiao, 1987) performed a theoretical analysis of the natural frequencies of a hyperbolic cooling tower shell considering geometric imperfections by using the perturbation method. The geometric imperfections were first considered as initial displacements to obtain the additional element stiffness matrix caused by meridional geometric imperfections. The authors found that the geometric imperfections increased the frequencies of the cooling tower. They also observed that the larger the range of imperfections, the more the frequencies were increased.

(Kaiser, et al., 1995) introduced the total Lagrangian formulation for axisymmetric solids in their earlier paper (1993) and later investigated in more detail its application to a series of sample structures (cylinders, pipes and cooling towers). Their formulation uses a cylindrical reference system to define the geometry, a Cartesian reference system for the displacement field. The displacement field in the circumferential direction was described by a Fourier decomposition. The authors performed analyses on several sample structures (spherical cap, cooling tower, cylindrical shell and a pipe in bending) to compare the formulation with Fourier decomposition shell models with conventional finite element formulations. The transformed displacements were related to the Cartesian system and the transformations expressed in a matrix form. The HLT element employed by the authors brought with it less computational effort devoted to the geometrical representation of the structure and more focused on the structural behavior as compared to the general three dimensional finite elements. The difference in the author's results from those of others indicated that the cooling tower dynamic problem had not been answered in detail.

(Busch, et al., 2002) summarized all the structural design aspects of the largest cooling tower at the time (using the Niederaussem cooling tower in Germany) as shown in Fig.2.1. They had considered that at a height of 200m, such a cooling tower can never be merely designed as an enlargement of the smaller ones, but would require careful and innovative design. The tower’s geometry was optimized to account for thermal design radius at the shell bottom, unperturbed steam flow radius at the top, practical bottom angle inclination and cost of reinforcement.

Openings in the shell for flue gas pipes were also considered in the design. Requirements to extend the cooling tower durability for a 55 year life time, limiting cracking and acid ingress into the concrete were considered by using an advanced high performance concrete (Acid Resistant High Performance Concrete: ARHPC). Fig.2.1 show the analysis results performed on the cooling tower.

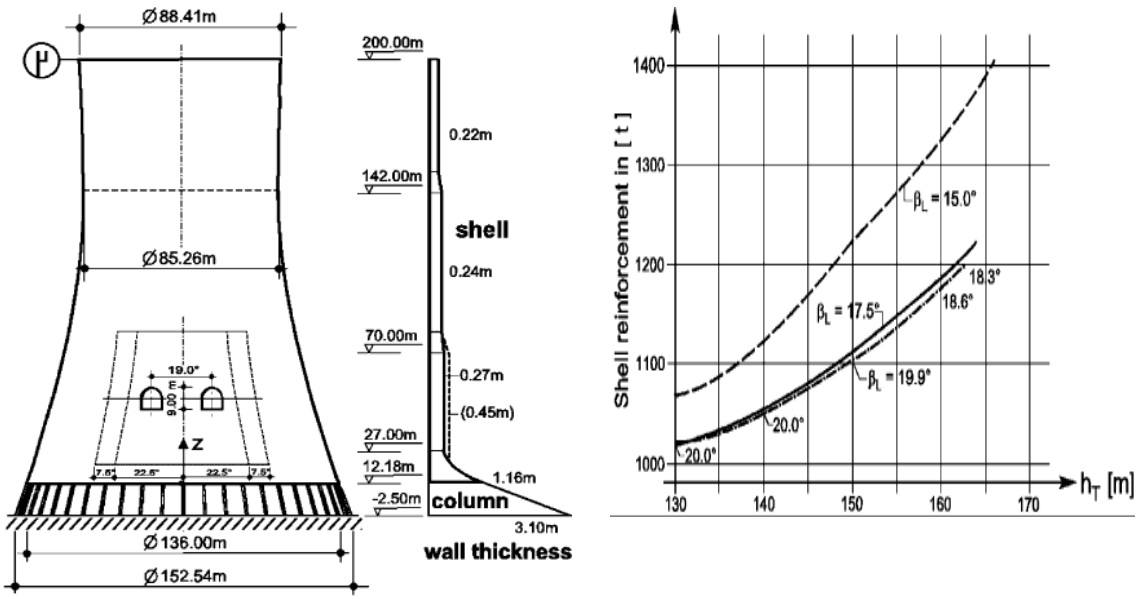

Figure 2.1 Overview of the cooling tower geometry, Shape-finding process: dependence of shell reinforcement on shell thickness (Busch, et al., 2002)

They found out that the lowest natural vibration modes and frequency with and without the flue gas openings were similar (see Fig. 2.1).

(Kim, et al., 2015) studied the p-version two-node mixed finite element for the prediction of free vibration frequencies and mode shapes of an isotropic shell of revolution, the cooling tower included. The two-node p-version mixed finite element was proposed for the free vibration analysis. Then the numerical performance of the mixed element was evaluated using several shells of revolution examples including the hyperbolic cooling tower shell of revolution. The cooling tower had been studied previously by Sen and Gould (1974). The shell was assumed to be fixed at the base and free at the top and all non-uniform variations in thickness were considered.

In their approach, the authors adopted the Hellinger- Reissner variational principal and the first-order Reissner-Mindlin shear deformation shell theory to solve the shell free vibrations equations. Some of the results of their study are shown in Table 2.1. They concluded that their study showed that the mixed element/s convergence and accuracy in the free vibration of shells of revolution was satisfactory. There was a good agreement between the results obtained by the authors and those by Sen and Gould (1974). The study confirmed that the mixed element finite element proposed can be applied credibly to practical shells of revolution with a very rapid convergence rate of the natural frequencies for the modes considered.

(Hara, 2015) evaluated the dynamic properties of a cooling tower under earthquake loading by considering a different column support system (I-column and V- column systems). The author introduced the numerical scheme under parallel processing to perform the dynamic evaluation of the cooling tower under seismic loading.

Table 2.1 Natural frequencies of the clamped-free hyperbolic cooling tower shell (Kim, et al., 2015)

Harmonic number n	Natural frequency (Hz)			
	Experiment	Sen	Kim (m=2) [10 element]	Kim (m=2) [15 element]
	188	168	167.58	167.56
4	130	130	129.94	129.71
5	-	122	122.31	122.21
6	157	143	143.56	142.82
7	177	161	161.95	161.40

2.2.2 Numerical studies

(Yang & Kapania, 1983) investigated various shell elements for the column support cooling tower in order to achieve on optimum finite element modelling for seismic response. Their intention was to understand the distribution of the dominating bending and membrane stresses as well as the vulnerable shell- column region of the shell by using the discrete column elements and the quadrilateral shell elements in the finite element model.

(Bhimaraddi, et al., 1991) studied the free-vibration response of a column supported cooling tower with ring stiffeners. They observed that this treatment had been performed for plates, cylinders, conical shells and spherical shells, but had not been extended to cooling towers.

Table 2.2 show some of the analysis results obtained. On comparing their results to those by Basu and Gould (1979) and Yang and Kapania (1983), the authors noted that there was good agreement between the results. There was no significant difference between the thick-shell and thin-shell results. This was noted to be due to the fact that both wall thicknesses were very small compared to the radii of curvatures. An increase in the frequency for the higher circumferential wave numbers (n > 3) and a decrease in the same for the lower circumferential wave numbers (n = 1, 2) was observed.

Table 2.2 Lowest natural frequencies of column-supported cooling tower (Bhimaraddi, et al., 1991)

Meridional mode Number(m) (1)	Basu and Gould (1979)(Hz) (2)	Yang and Kapania (1983)(Hz) (3)	Bhimaraddi, thin (Hz) (4)	Bhimaraddi, thick(Hz) (5)
1	2.336	2.333	2.3123	2.3085
2	4.119	4.156	3.9239	3.9236
3	7.056	6.952	7.2482	7.2450
4	_	_	8.2491	8.2474

The authors concluded that the provision of stiffening rings may not help increase the resistance of the cooling tower shell to seismic loads. The findings by the authors eliminated the premise that stiffening rings can be used to increase the load carrying capacity of cooling towers under seismic excitation.

(Lee, et al., 1995) presented an efficient numerical method to analyze the eigenvalue problem of large structural systems with multiple or close eigenvalues including the cooling tower. Their objective was to improve the numerical stability and (Asadzadeh, et al., 2014) studied the effects of the type and inclination of supporting columns of a cooling tower shell on its dynamic characteristics. The study analyzed the cooling tower shell as an assembly of layered non-linear shell elements comprising of different "reinforcement and concrete layers,".

They concluded that, for the I-type column, the cooling tower supported by vertical columns (I-90°) is flexible than when it is supported by inclined column supports. The structure's stiffness increases as the degree of inclination increases. The opposite was true

for the Λ-type columns: the flexibility of the whole cooling tower structure increases with a decrease in the degree of inclination of the column supports.

2.2.3 Experimental and field studies

(Shu & Wen-da, 1990) studied the dynamic properties of a cooling tower shell by considering the dynamic model of the shell and an infinite supporting soil system. Two methods of investigation were performed:

A finite element analysis of a cooling tower shell of revolution represented by high precision rotational finite elements, discrete column supports, and a soil medium represented by a dynamic boundary system (see Fig.2.2a).

An experimental investigation of a three part model consisting of a finite soil volume, a standard viscous boundary and an analytical energy absorbing boundary (see Fig.2.2 b).

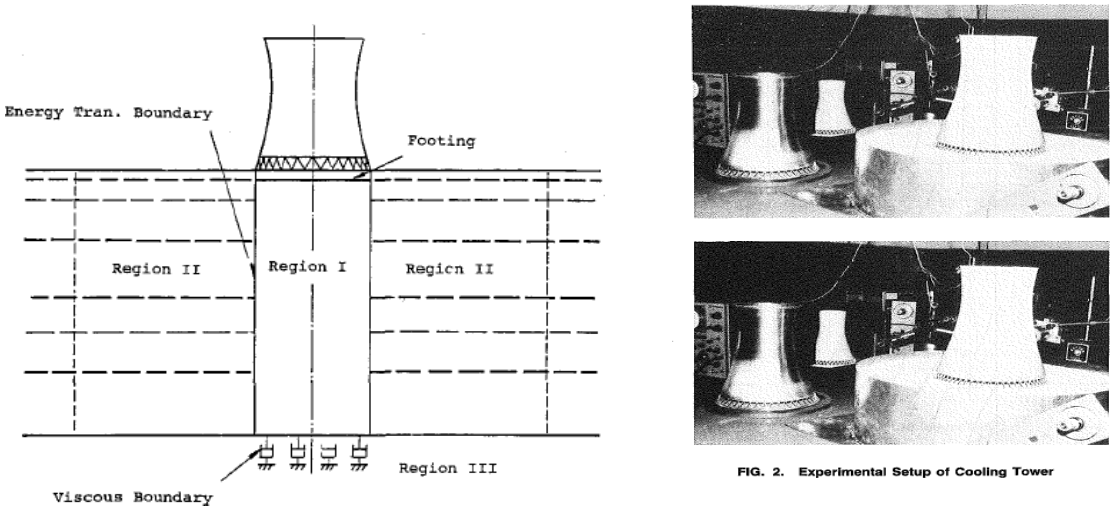

(a) (b)

Figure 2.2 (a) regions of soil and structure model, (b) Experimental model setup of cooling tower (Shu & Wen-da, 1990)

2.3 Dynamic Response - Forced Vibrations

2.3.1 Theoretical Studies

(Norton & Weingarten, n.d.) used a linear computer programme to evaluate the seismic response of different cooling towers with various asymmetric imperfections. They were concerned with the results of investigations by Weingarten et al (1973) and Schnobrich (1972) which had revealed that a significant response in higher circumferential wave numbers "did not exist." Their study used a computer programme to model one-half of the hyperbolic shell. The authors concluded that the achieved bending stresses were not a result of altering the beam bending modes but rather a result of modes other than the beam bending modes being excited. This meant that the cooling tower could have high bending stresses compared to membrane stresses when excited with an earthquake with a strong frequency. The study's findings raised an awareness for the need to increase reinforcement in regions of imperfections to allow for bending stresses that are higher than membrane stresses at certain seismic frequencies.

(Yang, et al., n.d.) studied the seismic response of the Paradise cooling tower in Kentucky (USA) using 3-D orthotropic quadrilateral flat plate finite elements. When comparing the fixed base versus column supported cooling tower, the authors found that the column supports reduced the natural frequencies of the cooling tower. This was in agreement with the observations by Gould et al (1974). The column top was observed to deflect significantly during seismic excitation. The study concluded that the fixed base assumption was therefore inadequate.

(Nasir, et al., 2002) performed a parametric study by treating the free vibration and seismic response of axisymmetric hyperbolic shell structures and examining the influence of thickness, height and curvature on this dynamic response. The study concluded the evidence that the first lateral mode of vibration was earliest in the tallest and thickest shell with the highest curvature. The tallest cooling tower was noted to experience some of the largest deflections and stresses. The higher stress resultants in models of the same height were observed in the thicker wall shells. The cooling tower shell was observed to be very sensitive to curvature by examining the significant changes in the meridional stress as the curvature was increased.

The results from the study confirmed that the first five circumferential modes of vibration and the first lateral mode all lie within the critical band of the dominant periods of most earthquakes. This finding can therefore be conveniently used to optimize the geometry of the hyperbolic cooling tower shell when designing for these structures in seismic areas.

(Kopenetz & Catarig, 2011) presented an efficient and simple free vibration analysis procedure for large cooling towers using bar type finite elements with inner nodes. They proposed that the cooling tower shell can be discretized as shown in Fig. 2.3.

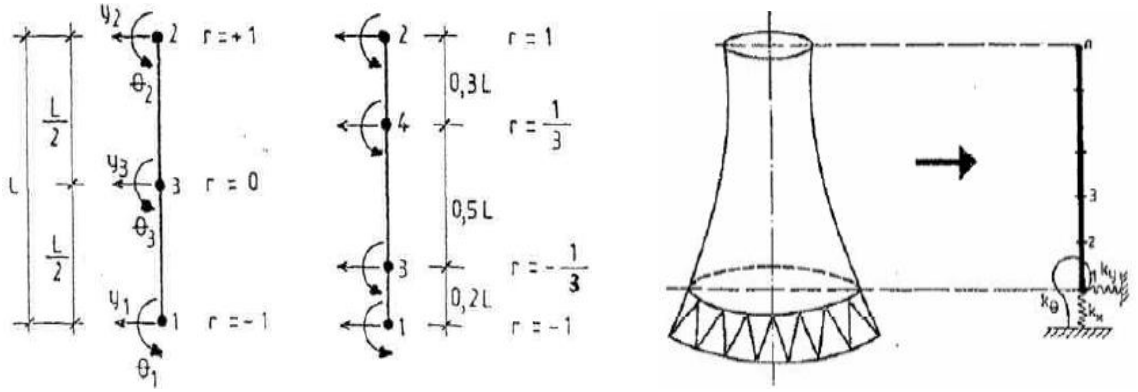

(a) (b)

Figure 2.3 (a) Cooling tower shell discretization, (b) Cooling tower structural model (Kopenetz & Catarig, 2011) respectively

2.3.2 Numerical Studies

(Julian, et al., 1983) acknowledged the earlier studies' (Albasiny and Martin, 1967; Ford, 1969) results that had showed that axisymmetric vertical flexibility of foundations reduces the cooling tower's capacity to carry wind loads by meridional membrane stresses thereby enhancing the development of circumferential bending moments along the whole height of the tower. Their study extended this finding to include the practical case of non-axisymmetric foundation stiffness. The authors concluded that the vertical flexibility of the foundation plays a significant role in the cooling tower behaviour and cannot be ignored in the design.

(Sabhouri-Ghomi, et al., 2006) investigated a cooling tower's dynamic behavior under seismic excitation using realistic horizontal and vertical ground acceleration data from recent earthquakes.

They concluded that the plastic hinges form mainly in the columns at junctions with other members where there are high stress concentrations. The plastic hinges in the shell were the last hinges to form. The hinge formation sequence depends on the nature of the earthquake. The inelastic dynamic response due to the plastic hinge formation reduces the stiffness of the cooling tower structure, reduced the applied base shear and increased the displacements. After the plastic hinges formation in the columns, the cooling tower would collapse under gravity loading

(Nangshineh, et al., 2013) investigated the behavior of cooling towers under seismic excitation by finding suitable support solutions that reduce earthquake effects. An iso-parametric solid element was used for the finite element modelling of the cooling tower. The investigation then focused on the cooling tower analysis with the hyperbolic cooling tower supported on either column supports on an annular raft on a fixed base and the effects of a ring beam support on the overall response of the cooling tower.

(Sahana & Sulaiman, 2013) performed a finite element static and dynamic analysis of a 125m high cooling tower by considering the influence of the shell thickness and size of opening in the shell on its behaviour.

(Li, et al., 2014) studied the modes and mechanisms of collapse of super-large cooling towers when subjected to accidental loads like vehicle collision, airplane impact, localised explosion and missile attack. The study concluded that only local damage occurred when the inclined columns suffered the truck collision, or a 200kg or less TNT equivalent mass explosion and the tower was still stable. Progressive collapse and different collapse modes were observed when the super- large cooling tower was subjected to large TNT equivalent mass explosions of 2000kg and 4500kg as well as an airplane impact. With the large TNT equivalent mass explosions, the inclined columns were severely demolished causing the entire structure to fall down. With the airplane impact, localized failure of the shell was induced causing the upper cooling tower shell to collide with the lower part due to gravity. The results obtained can be used to understand the collapse modes of super-large cooling towers when exposed to such accidental loads.

(Lin, et al., 2014) predicted ground motion accelerations caused by the collapse of a large-scale cooling tower under a strong earthquake. The authors concluded that the large-scale cooling tower may collapse under strong earthquakes with horizontal PGAs ranging from 0.35g to 0.45g. Moderate collapse induced ground vibrations may occur at horizontal PGAs ranging from 0.011g to 0.080g at 350m from the cooling tower. These vibrations were observed to attenuate with increased distance from the cooling tower. The results obtained from this study showed that the effects of collapse-induced ground vibrations should be seriously considered in the safety evaluation and planning of critical plants like nuclear power plants and related facilities.

2.3.3 Experimental and Field Studies

(Weingarten, et al., n.d.) Studied the effect of gravity loading on the seismic response of cooling towers. Their study performed free vibration analysis (natural frequencies and mode shapes) and forced vibration analysis of various size cooling towers using analytical and experimental methods. These were found to be in good agreement with the experimental results and the equations were solved using a finite element analysis method. They concluded that the natural frequencies obtained from the experimental investigation compared very well with those obtained from the finite element analysis. The dead load was noted to have a significant effect on the natural frequencies of the tallest cooling tower compared to the shorter ones.

(Sabhouri-Ghomi & Kharrazi, 2005) presented an analysis of the stability, non- linear behavior and the state of stresses of a hyperbolic cooling tower under seismic loading. The outcome of their analysis showed that there were no significant plastic deformations within the cooling tower shell elements. The first plastic hinges formed in the columns around the following regions:

- shell to column connections;
- column to foundation connections and
- Column to column intersections as shown in Fig.2.4.

They established that the buckling safety factor of the shell is not a concern under seismic excitation.

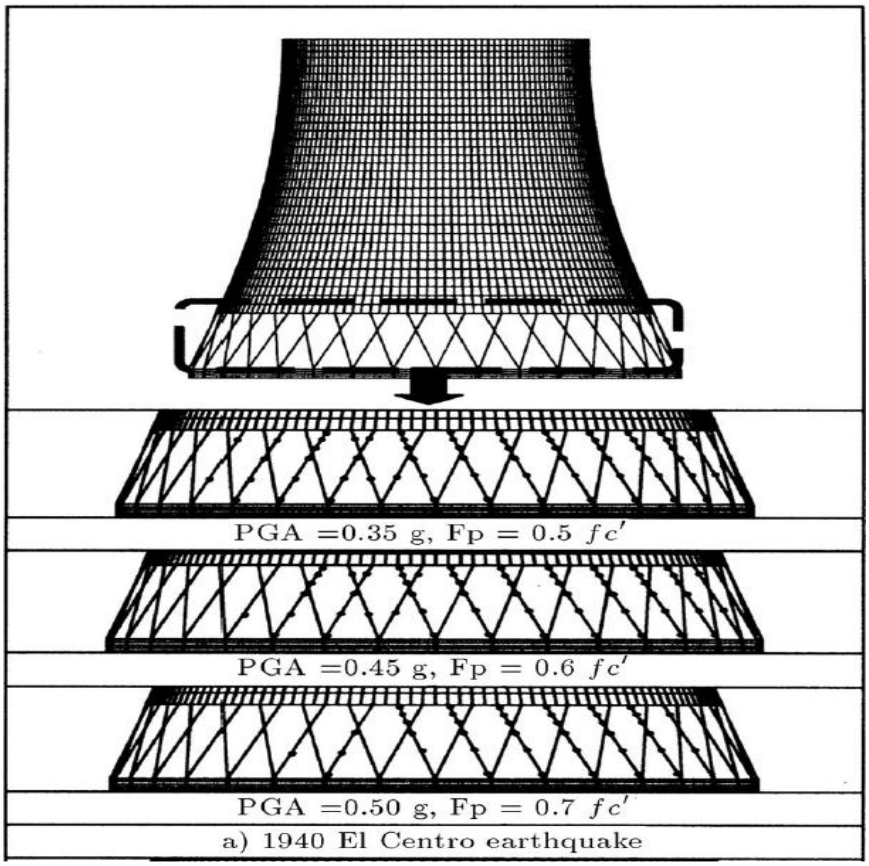

Figure 2.4 Plastic hinges formed in the finite element model (Sabhouri-Ghomi & Kharrazi, 2005)

(Qian-Qian Yu .et.al, 2016) Collapse-resistant performance of super-large cooling towers subjected to seismic actions using shaking table test was conducted on a 1/55 scaled reinforced concrete super-large cooling tower see figure. Structural dynamic responses corresponding to different levels of seismic actions were measured and analyzed. The structural weakness, collapse mode and failure mechanism were investigated. They found that the columns were the weakest part of the tower. Under strong-motion earthquake actions, the tower lost support after the columns failed and collapsed aslant overall.

(a) (b)

Figure 2.5 Scaled cooling tower: (a) scaled tower with templates removed; (b) scaled tower with weight blocks added.

The collapse mode of super-large cooling towers subjected to strong-motion earthquakes is classified as an inclined overall collapse. The tower failure in this experiment was mainly because columns failed as a result of large interlayer shear forces and deformations, and the shell structure lost its support.

2.4 Damage to Shell Structures Due to Earthquake

Although there has been a plethora of research on the response of the structures to earthquakes, there is still a dearth of information concerning the response of cooling tower shell systems to earthquake ground motions. Investigations of the damage to structures indicate that a lot of shell structures such as oil storage tanks, silos and large span roof shells have experienced considerable damages during past earthquakes. (Zama et al., 2006) reported damage to 30 tanks excited by long duration ground motion during the Tokachi-oki earthquake (M=8.0). This earthquake happened on 26 September 2003 in Tomakomai, in northern of Japan, with the damage occurring at a 225km distance from the epicenter. (Koketsu et al., 2000 and Sezen et al., 2006) have also reported similar damage to oil storage tanks during the 1999 Kocaeli earthquake in Turkey.

Damage was generally reported to be caused by liquid sloshing, excited by long period ground motions. Low frequency ground motions are most likely to be experienced in long duration earthquakes. Long period waves can cause damage at greater distances. Moreover, long period ground motions can cause more severe damage to large-scale structures as a result of their natural frequencies being closer to the low frequency spectrum of earthquakes having long durations. Sinking of 6 floating roofs of the tanks during the Tokachi-oki earthquake and more than 100 during Kocaeli earthquake have also been reported as being the result of sloshing. This damage suggests there is insufficient understanding of the behaviour of shell structures in earthquakes.

Cooling towers and stacks are other industrial structures that are vulnerable to severe earthquakes. Widespread damage to cooling towers and stacks have been reported during the Kocaeli earthquake. Two reinforced concrete heater stacks designed according to ACI 307 (ACI 1969), were destroyed during that earthquake. (Kilic and Sezen, 2003) have analysed these two stacks and found that the damage was because of the coincidence of the location of the reinforcing-bar splices and the region the most extreme earthquake induced flexural loading. Silos have also been damaged during past earthquakes. (Kawaguchi,1977) has reported that 12 circular cylindrical steel silos, used for wheat storage, each having 7.2 m diameter with 4.5 mm wall thickness at the top and 14 mm at the bottom, were heavily damaged by buckling collapse during the 1995 Hyogoken-Nanbu earthquake (M=7.2) in Japan. The increasing tendency to use shells in silos, tanks, stacks and many other structures, demands full understanding of the interaction between their geometric form and the seismic responses. There is currently little guidance as to how to prevent such catastrophic failures under earthquake loading.

2.5 Conclusion of the Literature Review

The literature review has been categorized into studies done on cooling towers in respect of their free and forced dynamic response when subjected to seismic excitation. The studies on dynamic response have revealed that openings and cut outs do not influence the lower natural frequencies and modes of the shell. A number of finite element models have been studied to obtain efficient converging models for the dynamic analysis of cooling tower shells subjected to seismic loading.

Addition of stiffening rings does not assist the seismic resistance of cooling tower shells. The modelling of the columns, foundations and soil-structure interaction plays a significant role in the results of finite element results on seismic dynamic response of the cooling towers.

The main focus of the studies has been on the dynamic property of cooling tower shells under seismic load. It was observed that generally equal attention has been focused on both wind induced vibration of cooling towers and their dynamic response to seismic excitation. However, less attention was observed on the form finding and geometrical parametric analyses. The most recent research trends were observed to focus on the wind induced vibration response of cooling towers as compared to seismic response. In addition, more attention is being given to the concrete deterioration, durability and repair methods of cooling towers.

Further attention should be focused on the vibration analysis of cooling towers when subjected to seismic loading. There is need to understand the dynamic behavior of cooling towers as their geometry is changed.

It is apparent that the gaps in the understanding of cooling tower behaviour are particularly on the effect of changing the shell geometry on the dynamic behaviour as well as finding shell forms that satisfy the required strength subjected to ground motion excitation.

In the light of the gaps, this research will focus on investigating the dynamic behavior of cooling towers in response to changes in shell geometry when the shell is subjected to seismic load.

CHAPTER 3 MATERIAL AND METHODS

3.1 Material

For this thesis the selected geometry and material from the previous research taken as reference model (J.Noorzeai 2005). The hyperbolic shell structure examined as a starting point, is based upon an existing cooling tower located at Stanwell Power Station, west of Rockhampton in Queensland Australia. Reinforced concrete has been considered with a unit weight of 25 KN/m^3, Poisson's ratio of 0.18 and elastic modulus of 31 GPa.

3.2 Geometry

The investigations by Gould (1977) provide interesting results for shape optimization of axisymmetric shell structures under axisymmetric loading of self-weight. This investigation has not only been verified but extended to axisymmetric hydrostatic and non-axisymmetric wind loading, during the project (Nasir et al.,2000a; 2000b). Gould (1977) considered geometric details of a hyperbolic curve generator, which is a negative Gaussian curvature, as shown in figure.

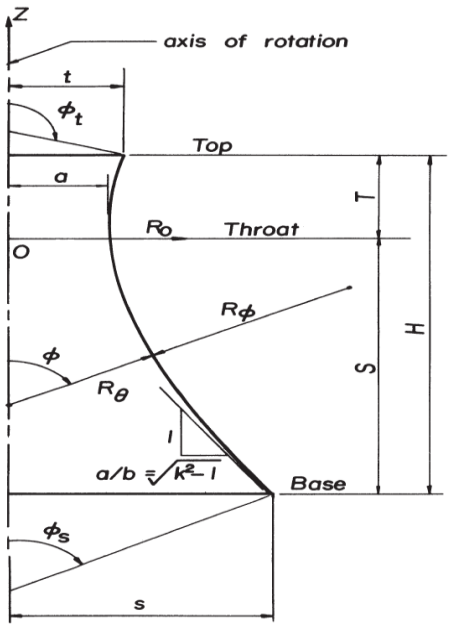

Figure 3.1 Hyperbolic shell of revolution-geometry (Gould 1977)

The equation of generated curve

$$\frac{r^2}{a^2}-\frac{Z^2}{b^2}=1 \tag{3.1}$$

where,

r = Horizontal axis i.e. radius of curvature of the parallel circle

Z = Vertical axis i.e. along the height of hyperbola with zero height at level 0.

a = Throat radius and 'b' is the characteristic dimension of the shell that may be evaluated by substituting the base co-ordinates (s, S) or the top co-ordinates (t, T) into Eq. (3.1) above, as shown in following Eq. (3.2);

$$b=\frac{aT}{\sqrt{(t^2-a^2)}}=\frac{aS}{\sqrt{(s^2-a^2)}} \tag{3.2}$$

The ratio a /b is the slope of the asymptote to the generating hyperbola, as can be seen in figure. The shape parameter

$$k=\sqrt{(1+\frac{a^2}{b^2})} \tag{3.3}$$

Deriving expressions for the principal radii of curvature in terms of the curvilinear coordinate ϕ, defined in the following equations;

$$R_\theta=\frac{r}{\sin\phi}=\frac{a\sqrt{(k^2-1)}}{[k^2\sin^2\phi-1]^{1/2}} \tag{3.4}$$

$$R_\phi=\frac{-a\sqrt{(k^2-1)}}{[k^2\sin^2\phi-1]^{3/2}} \tag{3.5}$$

$$\phi=\sin^{-1}\left\{\frac{r}{[a^2+k^2(r^2-a^2)]^{1/2}}\right\} \tag{3.6}$$

Values of ϕ in the first and second quadrant correspond to the lower and upper portions of the shell respectively, as defined in fig. Defining a non-dimensional meridional co-ordinate Φ Eq. (3.7) and variation of non-dimensional meridional stress n_ϕ Eq. (3.8) for different values of shape parameter k^2 Eq. (3.3), fig. 3.2 shows the meridional stress response along the height of axisymmetric shell structure when the shape deviates from cylinder {k^2= 1.05) to a hyperbola {k^2 = 1.50).

$$\Phi = \frac{\phi_t - \phi}{\phi_t - \phi_s} \tag{3.7}$$

$$n_\phi = \frac{N_\phi}{pa} \tag{3.8}$$

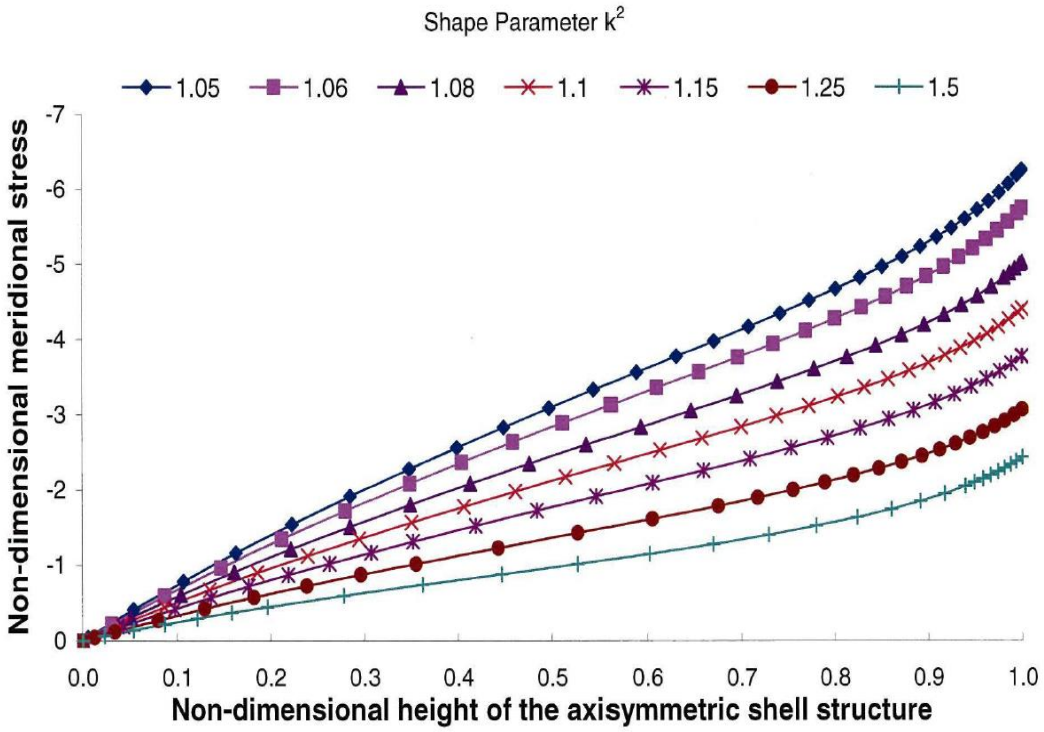

Figure 3.2 Meridional stress variation along the height of axisymmetric shell structure with change of meridian curvature (Gould, 1977; redrawn Nasir et al., 2000a)

Following nomenclature applies to the Eqs. (3.7, 3.8);

ϕ_t = Meridional angle at the top

ϕ_s = Meridional angle at the base

p = Self-weight of the shell structure

N_ϕ = Meridional stress

From the figure, it has been observed that and thus concluded that the self-weight (typical axisymmetric load) meridional stresses reduce with increase in curvature i.e. as the axisymmetric shape deviates from the cylindrical shape to a hyperbolic form, there is a decrease in the induced stresses.

In this thesis, geometric dimension of the reference model also from stanwell cooling tower Australia based on (J.Noorzaei, 2006) and the parameter is tabulated as shown the table 1 below and the model also present here as shown in the figure.

Table 3.1 Geometric parameter of reference model

Description	symbol	Value(m)
Height above throat level	Z_H	24.090
Height below throat level	Z_U	91.260
Top diameter	d_C	55.070
Throat diameter	d_T	50.608
Shell base diameter	d_L	96.582
Column diameter	-	0.700
Number of column pairs	-	45.00
Column height	Z_C	6.950
Wall thickness lintel	h_1	0.700
Wall thickness between lintel and cornice	h_2	0.170
Wall thickness cornice	h_3	0.500

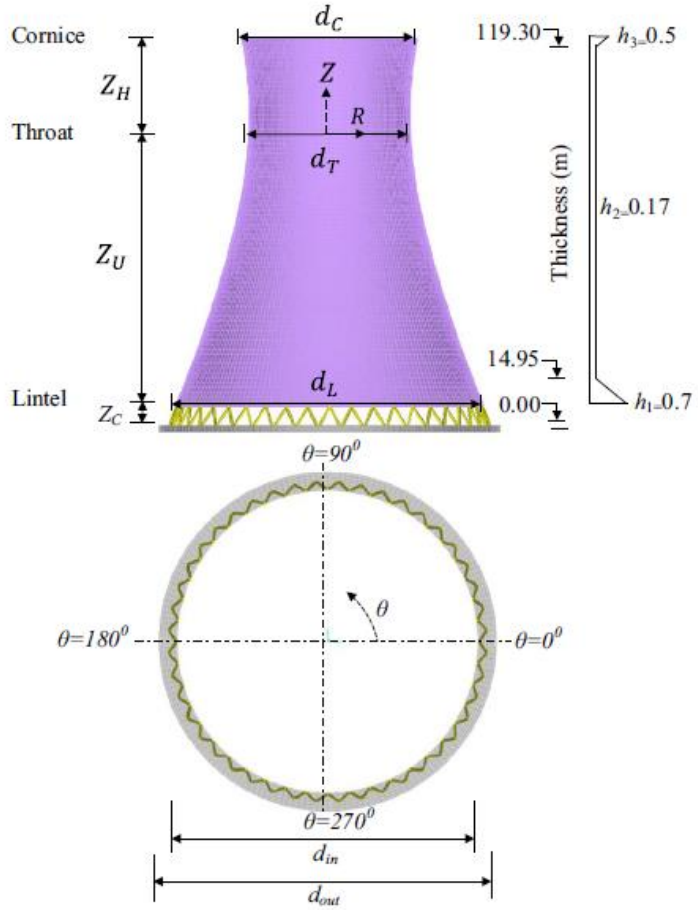

Figure 3.3 Hyperbolic cooling tower reference model

3.3 Parametric Study

For the parametric study, the influence of some characteristic parameters of cooling towers such as height- to-throat-radius ratio (H/d_T), radius-to-thickness ratio (R/t), height-below-throat-to-height-above-throat ratio (Z_U/Z_H) and the shape parameter (κ) on the dynamic behavior of cooling tower under seismic load were investigated and the connection between column and foundation assumed to be rigged. For detail of selected geometry, see table in appendix A table A1.

First of all, the meridional curvature of bottom or upper part of the cooling tower from throat level is a critical geometrical parameter to be investigated. For this purpose, (d_L) is kept constant at 96.582 m and the neck of the tower base diameter ratio (d_L/d_T) are 1.75, 2.00, 2.25, 2.50 and 2.75 neck diameter (d_T) was determined and five different solutions made. Here the increase in d_L/d_T ratio increases the curvature.

The elevation views of the cooling towers with changing throat diameters are shown in Fig.3.4.

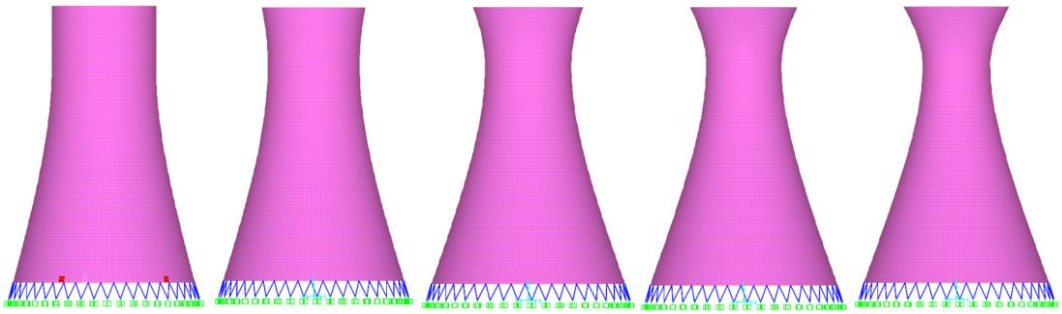

d_L/d_T=1.75 *d_L/d_T=2* *d_L/d_T=2.25* *d_L/d_T=2.5* *d_L/d_T=2.75*

Figure 3.4 Cooling tower views with varying throat diameter or curvature

The influence of wall thickness on tower behavior in the third stage is considered by changing radius-to thickness ratio, R/t keeping radius constant. The ratio of shell radius to shell thickness (R / t) 50, 75, 100, 125 and 150 will be linearly varying through the tower height. The thickness (t) was calculated and five different analyzes was performed. As can be seen, with increasing R / t ratio shell thickness is reduced.

Then the same cooling tower effect of slenderness was investigated. while keeping the throat diameter d_T 50.608m and the height-below-throat-to-height-above-throat ratio (Z_U/Z_H = 4) constant. Additionally, a constant wall thickness with 50 cm were assumed. The ratio of tower height to neck diameter (H / d_T) 2.0, 2.5, 3.0, 3.5 and 4.0 as the tower height (H) and five different analyzes were performed. Increasing H / d_T ratio it means increasing the fragility. And the elevation views of cooling towers for these ratios are depicted in Fig. 3.5.

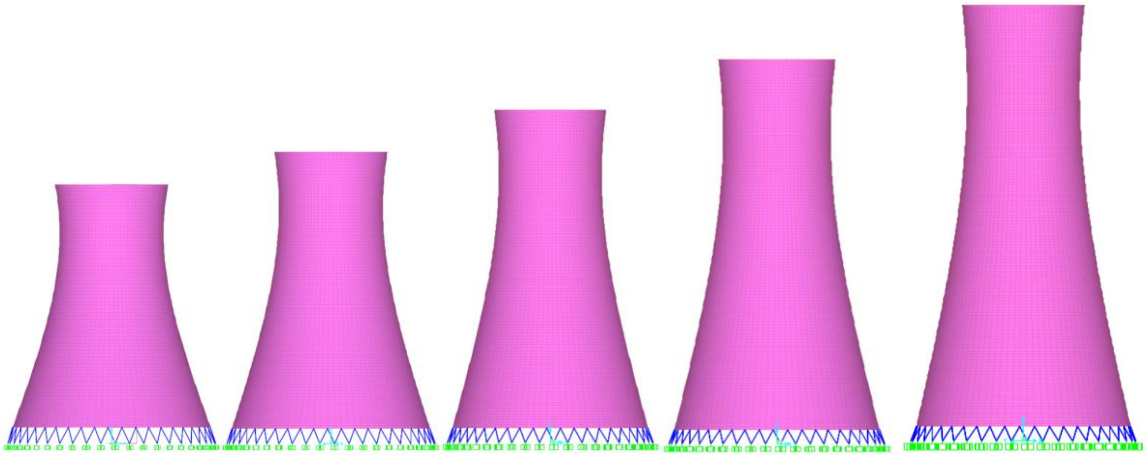

H/d_T=2 *H/d_T=2.5* *H/d_T=3* *H/d_T=3.5* *H/d_T=4*

Figure 3.5 Cooling towers views for various slenderness ratios (appearance)

Finally, The level of throat is one of the characteristic parameters of cooling towers. This parameter is defined by the height-below-throat-to-height-above-throat ratio (Z_U/Z_H). To investigate the effect of throat level, the tower height H ($Z_U + Z_H$) is held constant and the ratio of Z_U/Z_H is altered between 0, 1, 2, 3 and 4 while keeping all other parameters constant. (Z_U / Z_H) ratio is zero for neck level peak. The elevation views of the cooling towers with changing throat levels are shown in Fig. 3.6.

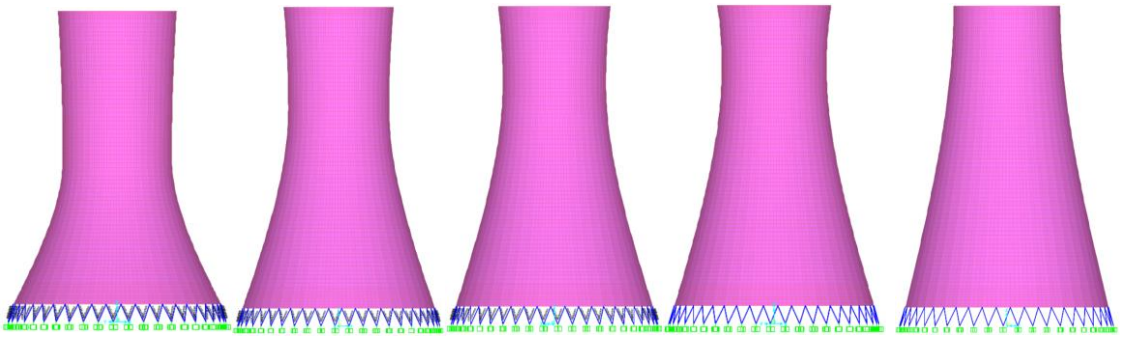

Z_U/Z_H=1 *Z_U/Z_H=2* *Z_U/Z_H=3* *Z_U/Z_H=4* *Z_U/Z_H=0*

Figure 3.6 Cooling tower views for various throat levels

3.4 Earthquake Loading

Possible loading conditions are dead load, wind load, earthquake load, temperature variations, construction loads, and settlement for a hyperbolic cooling tower. In the scope of this study only earthquake loads are considered. Ground motions generate the earthquake loading on hyperbolic cooling towers. The circumferential responses become anti-symmetric for uniform horizontal motion. The magnitude of earthquake forces is a function of the mass of the shell and the ground acceleration. Seismic responses of the hyperbolic cooling tower are investigated for acceleration-time records of different earthquake ground motion matching with target response spectrum provided on the design specification code **ES EN 1998-1:2015.** For this study, the target response spectrum is type 1, soil classification "c" and the peak ground acceleration is selected based on zone 5 as per code provision. Before I have selected seismic zone, literature revision was performed about the possible area of these nuclear and power plants constructed in our country that has been vulnerable to ground motion. Based on the revision one of the very interesting site higher amount of coal production located 165km away from Addis Ababa to Dessie road near Tarmaber tunnel at mush valley. So this site is used as the reference for the current study because the area is located in the Great Rift Valley and higher seismic ground motion expected.

3.5 Method for Scaling or Matching Ground Motion Records

A summary of the two design specifications used in this study is presented below. Both design specifications require the computation of a multiplication factor to apply to the chosen time history to ensure a match to the target spectrum in the period range of interest. However, this factor is computed by different ways depending on the standard or code considered.

3.5.1 U.S.A. Standard (ASCE/SEI 7-10)

ASCE (2010) requires the use of at least three ground motions. Each ground motion shall consist of pairs of appropriate horizontal components that shall be selected and scaled from recorded events. The selected ground motions shall have magnitudes, fault distance, and source mechanisms consistent with the expected maximum earthquake considered in the analysis.

Soil profile similarities are not required explicitly by this standard. Appropriate simulated ground motion pairs can be used to make up the total number of ground motions when the required number of recorded ground motions is not available.

The square root of the sum of the squares (SRSS) of the 5% damped response spectrum of each ground motion must be computed from the scaled pairs that form the record. The same scale factor shall apply to both pairs of the record, i.e., each record has a unique scale factor. The scale factor is determined by the criterion that the SRSS of the response spectrum of each record shall not be less than the target spectrum in the period range of interest defined by ASCE (2010). The period range is specified as being between 0.2 *T1* and 1.5 *T1,* where *T1* is the fundamental period of the structure in the direction analyzed.

When seven or more ground motions are used to perform the analysis, the average response will be considered for design purposes. If less than seven ground motions are used, then the maximum response will be considered.

3.5.2 ES EN 1998-1:2015

This design specification requires the use of a set at least three pairs, regardless of their origin. The records shall consist of both horizontal components and a vertical component when this is required. The records that make up the set shall be consistent with the magnitude and other relevant features of the seismic event considered.

The average of the 5% damped elastic spectrum, calculated from all time histories, should not be less than 90% of the target spectrum in the period range of interest. The period range of interest defined by Eurocode 8 is between 0.2 T1 and 2 T1, where T1 is the fundamental period of the structure in the direction of application of the motion. It should be noted that this procedure, contrary to the previous one, does not provide a specific method to compute the scale factors for the records. The requirement established by Eurocode 8 can be fulfilled in several ways. Even an single unique scale factor for all the records can be used if the average of the 5% damped elastic spectrum of all time histories meets the requirement. Iervolino et al. (2008) realized this issue and proposed additional conditions on choosing ground motions to be utilized for time-history analysis. Katsanos et al. (2010), present a complete review of the state of art of the selection of records for time-history analysis.

They confirmed that there is a high variability in the spectral acceleration when real unscaled records are used following the procedure given by Eurocode 8. As an additional requirement, the average spectral acceleration, calculated from the individual, time histories, at a period essentially equal to zero has to be larger than the value of the target spectrum at the same period.

It is recommended that seven or more ground motions be used and the average response taken for design purposes. If less than seven ground motions are used, then the maximum response should be considered.

3.6 Ground Motion Records and Target Spectrum

A set of three different earthquake records are utilized in the time-history analysis. The earthquakes selected are shown in Table. The ground motions were selected according to the recommendations given by ASCE (2010) and Eurocode 8/ ES EN 1998-1:2015 and are appropriate for a site in Tarmaber typically mush Valley, Ethiopia. ES EN 1998-1:2015 will be used to determine the design spectrum for this site.

Horizontal components of each earthquake are used in this study. ASCE (2010) and Eurocode 8 require at least three records to utilized before the maximum response can be considered for design purposes.

Table 3.2 Earthquake ground motion records

Soil classification C						
Earthquake	Date	Station	Magnitude (Mw)	Distance from fault (km)	PGA (g)	Vs30 (m/sec)
Duzce	11/12/1999	Duzce	7.140	6.580	0.404	281.860
Kobe	1/16/1995	KJMA	6.900	0.960	0.629	312.000
North ridge	1/17/1994	N-Hollywood	6.690	12.510	0.309	326.470

All the ground motions records were matched to the target spectra defined in the previous section by using the SeismoMatch software given by the design specifications described in previous Section. Fig.3.7 shows the unscaled 5 % damped response spectra of the records and the target spectrum for both site classifications. Both horizontal components are shown in Fig.3.7.

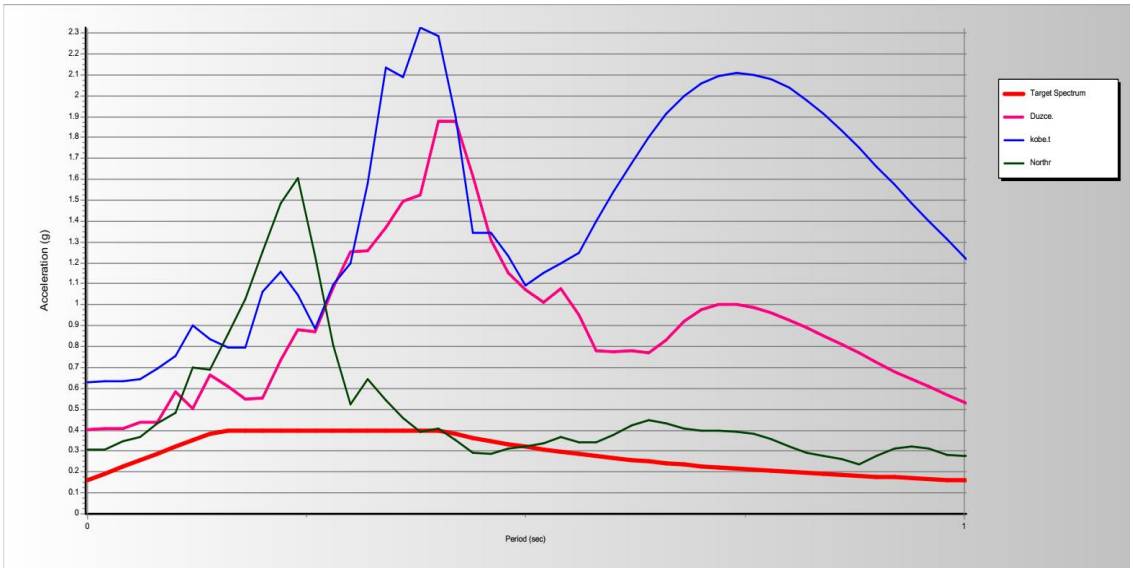

a) ground motion spectra and target response spectrum before matching

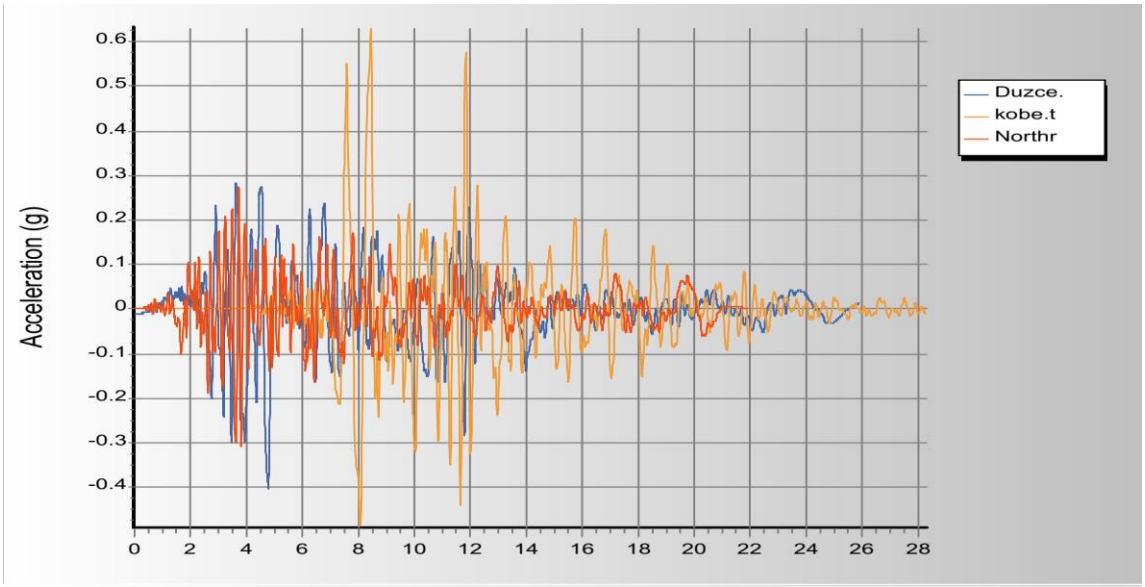

b) actual ground motion record for corresponding soil class C

Figure 3.7 Response spectra and time history ground motion records

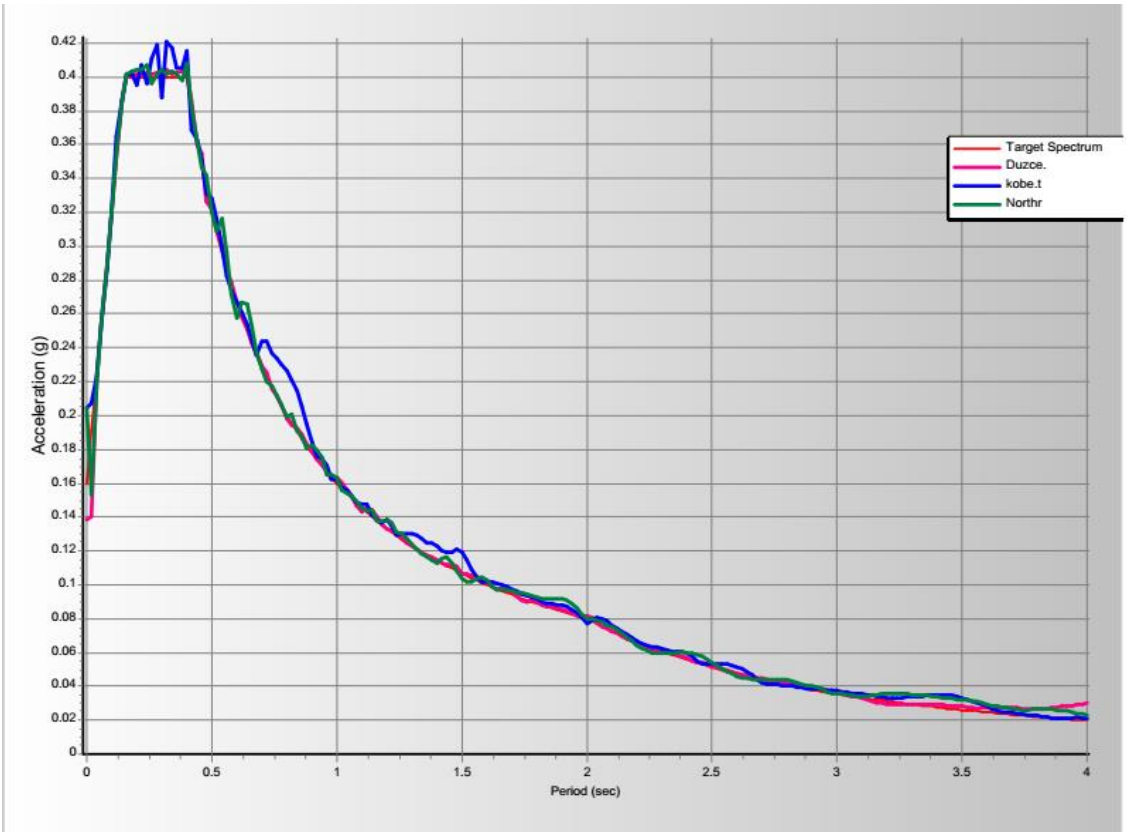

a) ground motion spectra and target response spectrum after matching

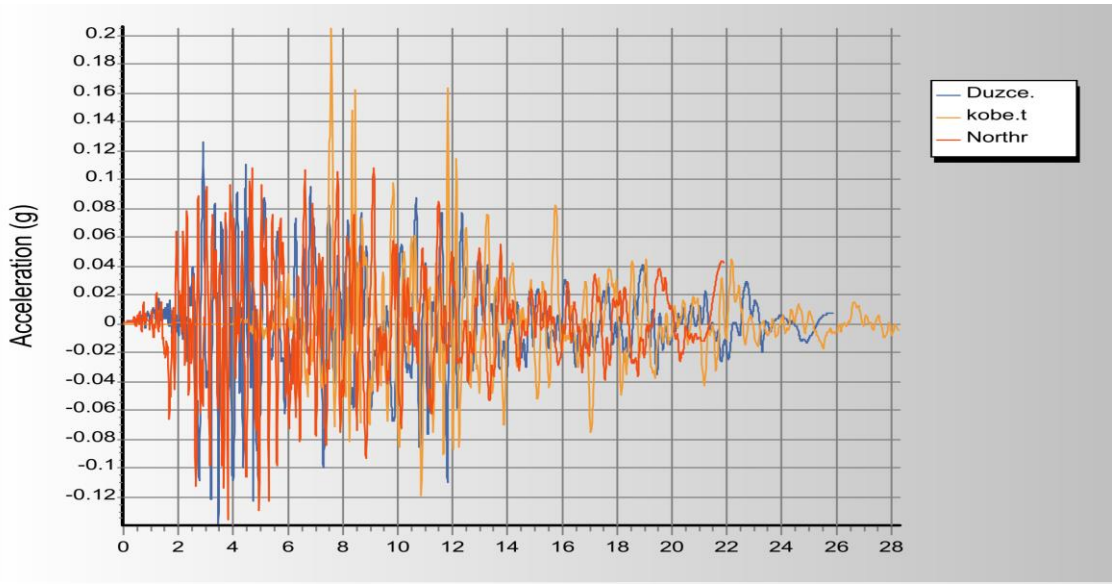

b) artificial ground motion record for corresponding soil class C after matching

Figure 3.8 Matched spectra and time history ground motion

3.7 Finite Element Modeling

Earlier dynamic analysis of cooling towers were also conducted for the case of fixed base by the use of membrane theory. The bending theory of thin elastic shells was later successfully applied to the free vibration analysis of cooling towers with fixed bases. Among the methods of analysis are numerical integration method, finite difference method, and finite element method with the use of rotational ring-type shell elements. The finite element method is chosen to analyze the cooling towers, the most exact way to model the supporting columns appears to be modeling each column as a distinct element through the use of column finite elements with an exact stiffness formulation. To accomplish this, however, one cannot use the rotational shell finite elements since the nodal circles cannot be connected to the column joints. The quadrilateral shell finite elements must be used instead. The capability of the quadrilateral shell finite elements in predicting natural frequencies of cooling towers is first evaluated through an example of a fixed-base cooling tower. Results for frequencies compared well with previously reported results. Modeling and analysis of the tower is done by SAP2000 package Ver. 20.2. The supporting columns have been modeled as 2-noded line elements having 6 degrees of freedom at each node. The cooling tower shell has been modeled as the quadrilateral element. This element is the 4 nodded shell elements which permits the full shell behavior of the tower which is a combination of membrane and plate behavior and supports all forces and moments except the drilling moment. This element has six degrees of freedom (with three translational and rotational degrees of freedom) at each node (Ibrahimbegovic and Wilson 1991). The use of the full shell behavior (membrane plus plate) is recommended for all three- dimensional structures (SAP2000 Analysis Reference 2009). The three-dimensional analysis has been carried out. Model used for this study presented in the previous section (parameter for study). The detailing of modeling and plot of the geometry of the cooling tower is presented in Appendix A table A2, figure A1 and A2, respectively.

3.8 Verification of Software

Verification of software model were performed using analytical and pervious established solution for static and dynamic load respectively. A case study of an already established solution for dynamic free vibration response of a hyperbolic cooling tower was considered for numerical model verification in the present study. Nasir *et* al. (2001 a) had earlier computed the natural frequencies using finite element method. In this study, a computer aided finite element model is Analyzed on Sap2000 V 20.2 using geometry, material properties & boundary conditions as adopted by Nasir *et* al. (20001 a).

The structure has a total height of 121.5m with base, throat and top radii of 45.30m, 27.89m and 29.02m respectively. The throat is located 95.6m above the base of the shell. A constant shell wall thickness of 240mm and fixed base support conditions are considered in the finite element model. Reinforced concrete has been considered with a unit weight of 25 KN/m^3, Poisson's ratio of 0.2 and elastic modulus of 39 GPa.

Quadrilateral three-dimensional isotropic shell elements are used to model the shell. This element uses six degrees of freedom (three displacement components and rotations) per node, and thus typically models thin shell structures. An optimum mesh size is adopted after convergence study. The top edge of the shell structure is free to translate and rotate in all directions, while the base is completely fixed i.e. no translation and no rotation; in agreement to Novozhilov (1959).

Table 3.3 Finite element model verification; comparison of present results with those previously stablished solutions

Methods of solution	Periods of vibration (s)					
	1	2	3	4	5	6
Nasir et.al	0.723	0.668	0.662	0.596	0.549	0.294
this study	0.723	0.667	0.663	0.595	0.549	0.294
Relative error (%)	0.000	0.150	0.150	0.170	0.000	0.000

Table 3.3. gives a comparison of the natural frequencies obtained from the present study and those obtained by Nasir *et* al. (2000 a). Same geometric and material properties have been considered in the two cases. As can be seen, the results are quite encouraging and

provide confidence in the subsequent analysis. A convergence study is carried out to determine the required number of elements to provide an acceptable level of accuracy in the modal analysis. Static load verification of software by using the Gould(1976) formulation.

The principal radii of curvature are given by equations (3.4) and (4.5), and the loading components are $q\phi = q \sin\phi$ and $qn = - q \cos \phi$. Assuming a stress-free top edge, $N\phi(\phi t) = 0$, and q = constant (uniform thickness) the meridional and circumferential stress can be;

$$N_{\phi}(\phi) = \frac{qa\left[k^2 \sin^2 \phi - 1\right]^{1/2}}{\sin^2 \phi \sqrt{\left(k^2 - 1\right)}} \left[\zeta_1(\phi) - \zeta_1(\phi_t)\right]$$

in which the integrated function

$$\zeta_1(\phi) = \frac{-\cos\phi}{2\left[k^2 \sin^2 \phi - 1\right]} + \frac{1}{4k\sqrt{\left(k^2 - 1\right)}} \ln\left(\frac{\sqrt{\left(k^2 - 1\right)} - k\cos\phi}{\sqrt{\left(k^2 - 1\right)} + k\cos\phi}\right)$$

The circumferential stress resultant N_{Θ} is computed as

$$N_{\theta}(\phi) = \frac{a\sqrt{\left(k^2 - 1\right)}}{\left[k^2 \sin^2 \phi - 1\right]^{1/2}} \left[-q\cos\phi + \frac{N_{\phi}(\phi)\left[k^2 \sin^2 \phi - 1\right]^{3/2}}{a\sqrt{\left(k^2 - 1\right)}}\right]$$

Using the above analytic equation and SAP2000 FEM, numerical and FEM solution computed, graphically presented and compared. ***(See the plot data in the table Appendix C)***

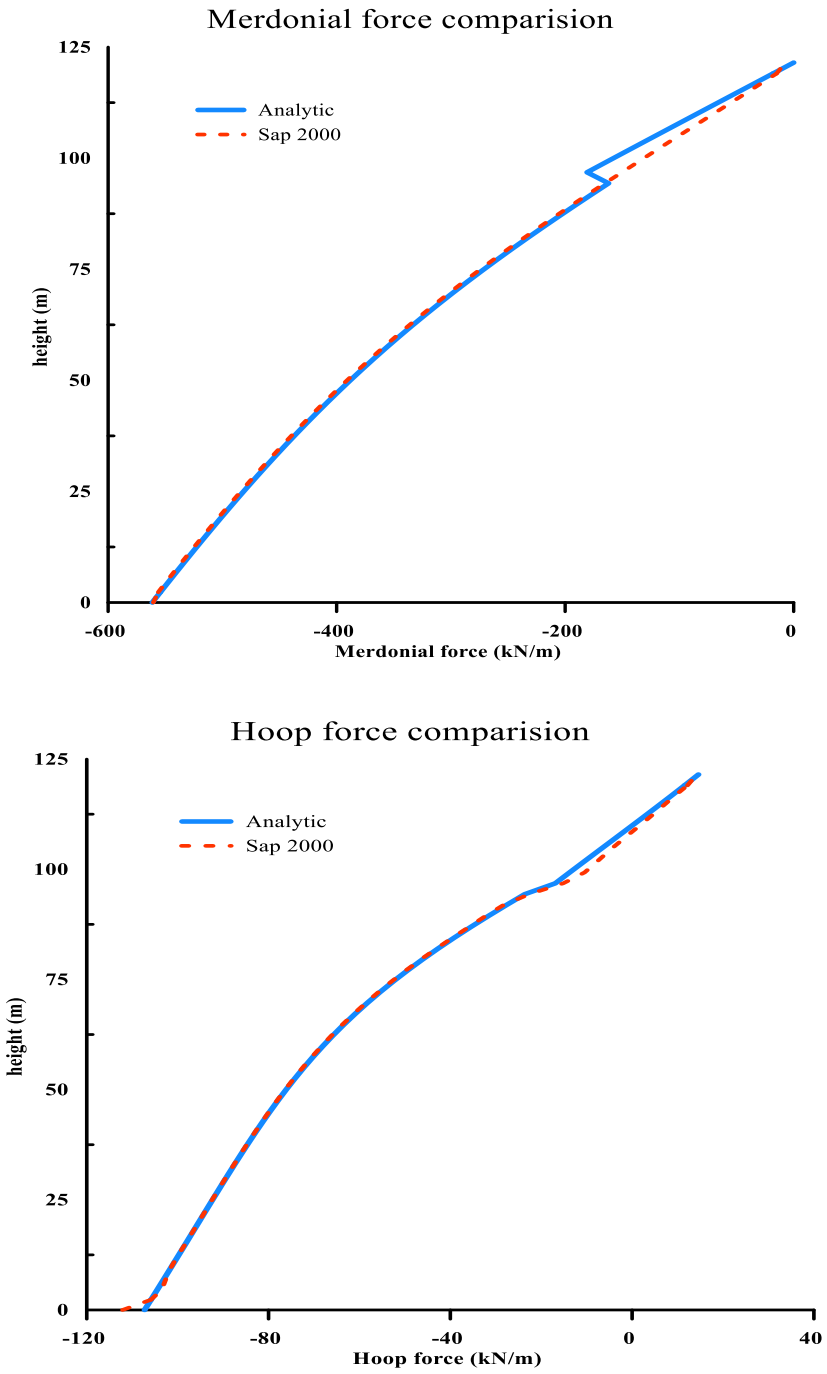

Figure 3.9 Comparison of analytic solution and sap2000 software

From the graph presented above software and analytic solution very good agreement, so using that FEM package software for analysis is adequate.

3.9 Dynamic Analysis Method

The differential equation Eq. (3.9) governing the response of multiple degree of freedom systems to earthquake induced motion are:

$$[M]\{\ddot{u}\}+[C]\{\dot{u}\}+[K]\{u\}=-[M]\{\ddot{u}_g\} \quad (3.9)$$

Here, the stiffness matrix of the system [K], [C] the damping matrix and [m] is the mass matrix of the system. u, $\dot{u}$, and $\ddot{u}$ horizontal displacement, the first derivative of the horizontal displacement over time and second derivative of horizontal displacement over time respectively and $\ddot{u}_g$ is the acceleration of earthquake. The damping matrix C would not be needed in modal analysis of earthquake response; instead modal damping ratio suffice and their numerical values can be estimated as Eq. (3.10) for the n^{th} diagonal element for generalized modal damping (Chopra, 2007):

$$C_n=\zeta_n(2M_n\omega_n) \quad (3.10)$$

3.9.1 Modal Dynamic Analysis

Modal dynamic analysis is a linear perturbation procedure, used to analyze the transient linear dynamic problems using the modal superposition method. It gives the response of the model subjected to an external time dependent loading as a function of time. This procedure derives the response of the requested numbers of the modes of the system. Modal amplitude of each mode is integrated through time, and then the total response is found by combination of these modal responses. This method produces accurate results for linear systems with adequate numbers of modes being selected, which is a small portion of the total modes of the finite element model. The reason for accuracy is because the integration operator used is exact when the external load varies in a piecewise linear manner with time. However, the choice of time increment should be consistent with the time increment of the external loading. The damping coefficient can also be considered constant (5%) for the whole range of participating
frequencies as it is assumed for this study.

3.9.1.1 Equation of Modal Dynamic Analysis

As mentioned earlier the modal dynamic response provides time history analysis for linear problems. The external dynamic force is given as a function of time, assuming that the variation of the magnitude of the excitation within each increment is linear. The total response is based on the combination of responses of its participating modes, in which each mode can be considered as a single degree of freedom. Each uncouple one degree of freedom system, should satisfy the equilibrium equation at time t

$$\ddot{q} + 2\xi\omega\dot{q} + \omega^2 q = p_t = p_{t-\Delta t} + \frac{\Delta p}{\Delta t}\Delta t \qquad (3.11)$$

Where ζ is the critical damping ratio, q is the amplitude of the response in this mode, P is the magnitude of the modal loading, ΔP is the change in P over time increment (Δt), and ω is the natural frequency. It is assumed that the excitation varies linearly within each time increment.

3.9.2 Response Convergence with Mode Numbers

Of practical importance are the numbers of modes required for accurate prediction of displacement, acceleration, stress, etc., for a specific geometry of shell. In order to explain the reason for requiring such a large number of modes in the analysis of stresses, the ratio of participating mass to the total effective mass of the structure is checked and compared with the requirement of Uniform Building Code (UBC), 1997 and Eurocode 8.

The UBC requires the number of modes in the modal analysis to be selected such that their participating mass is at least 90% of the total effective mass. Eurocode 8 demands either the participation of mass to be 90% of the total effective mass or inclusion of every mode with effective masses greater than 5% of the total mass. Although in the present case the participating mass reaches 90% of the total effective mass of the shell after 250 modes, and hence satisfies the requirement of the UBC and Eurocode 8

CHAPTER 4 ANALYSIS RESULT AND DISCUSSION

4.1 Introduction

In this thesis, a parametric study is performed to interrogate the relationship between the dynamic response due to ground motion of a hyperbolic cooling tower with its geometrical parameters of slenderness, neck level, thickness and curvature. The various geometrical parameters are represented as parametric ratios in order to cover a wider range of cooling tower geometries. Some interesting trends are observed when the results are plotted against the various geometrical parameters and their ratios. All analysis results are represented graphically gained from the horizontal or circumferential position at 0^0 except for shear force at 90^0 along the height of the towers. The graph shown here the result from the analysis by inputting the ground motion of Duzce Earthquake. The Kobe and Northridge result output presented in appendix B plot together correspondingly.

N.B. all plots were made assuming that the lateral load or earthquake load applied at x and y direction and degree of application was 0^0.

4.2 Horizontal displacement

Maximum horizontal displacement as we can see from the shape it is formed at the peak level as expected and its results are presented graphically as shown in the Fig. 4.1 below. d_L/d_T ratio increase the tower top point displacement and also increase from d_L/d_T=2. Obtained maximum displacement 3.69, 3.59, 4.01, 4.38 and 4.80 cm, respectively. When you compare smallest and largest displacement a large value increment, by 33.7%. As the diameter of the neck decrease, horizontal displacement will increase and stiffness reduced.

The slenderness will increase H/d_T ratio increase and displacement depending on this ratio; the maximum horizontal displacements were 3.72, 6.67, 7.6, 16.18 and 17.96 cm. As the height of the tower increases, the change in the displacement observed between the largest and smallest values is 382.8%.

If the ratio of R / t is increased, horizontal displacements are decrease and behaved oppositely. The maximum values at peak point obtained were 5.43, 4.35, 4.03, 3.72 and

3.20 cm respect to ratio of R/t. Consider the smallest and largest values the change were about 69.69%.

When Z_U/ Z_H ratio is 1 maximum displacement was observed and for the ratio of Z_U/Z_H increase the displacement reduced continuously. Here the maximum displacements obtained were 3.49, 5.39, 4.30, 4.38 and 3.72 cm, therefore the largest and smallest change in value is in the order of 54.4%.

Slenderness and thickness effects on Hyperbolic cooling towers are more dominant and decisive than other variable when considering horizontal displacement.

Table 4.1 Maximum horizontal displacement U1 (cm)

Case	d_L/d_T (curvature effect)	U1 (cm)
1	1.75	3.69
2	2.00	3.59
3	2.25	4.01
4	2.50	4.38
5	2.75	4.80

Case	H/d_T (slenderness effect)	U1 (cm)
1	2.00	3.72
2	2.50	6.67
3	3.00	7.60
4	3.50	16.18
5	4.00	17.96

Case	R/t (thickness effect)	U1 (cm)
1	50	5.43
2	75	4.35
3	100	4.03
4	125	3.72
5	150	3.20

Case	Z_U/Z_H (throat level effect)	U1 (cm)
1	0	3.49
2	1	5.39
3	2	4.30
4	3	3.80
5	4	3.72

Note: the plot data were recorded at 0 degree and the application of the direction of the earthquake load in the global x and y direction at 0^0.

As can be seen the plot the curvature effect indicates that the displacement may cause failure near the neck level because it is weak point of the tower and rigid below and top part of the structure.

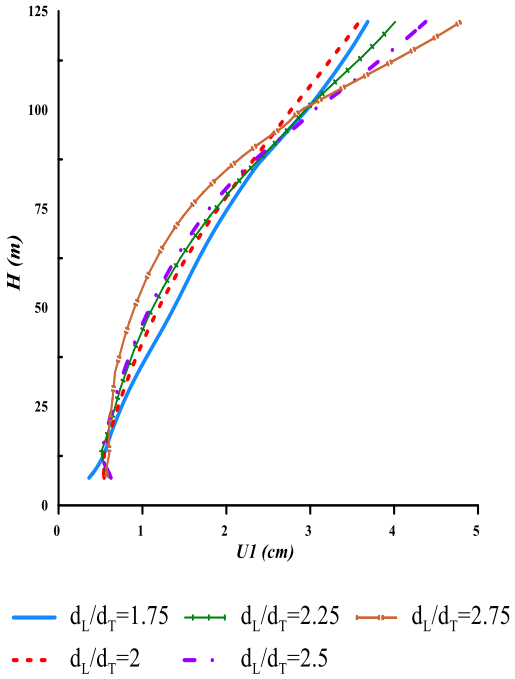

a) Curvature effect

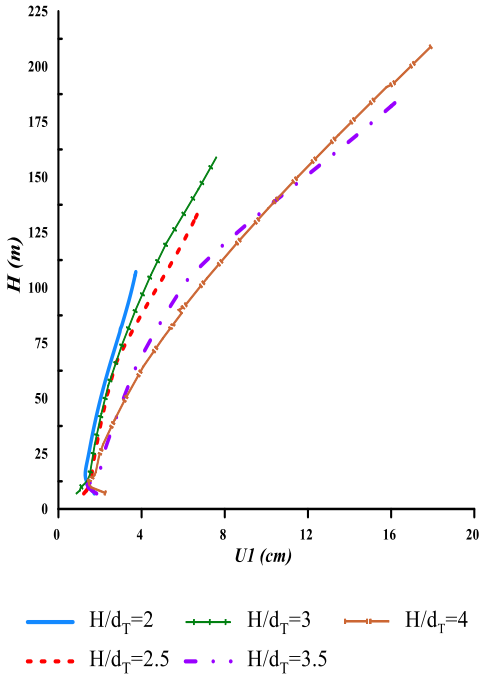

b) Slenderness effect

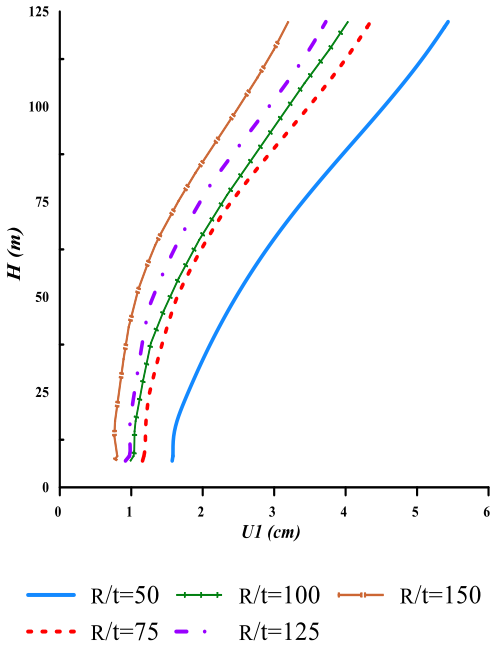

c) Thickness effect

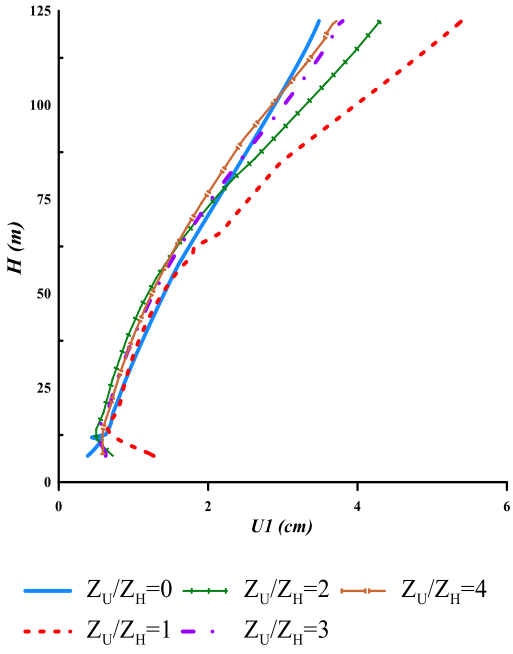

d) Throat level effect

Figure 4.1 Vertical variation of the horizontal displacements

4.3 Hoop, Meridional and Shear Forces along Height

Internal forces and moments in SAP2000 software local axes 1, 2 and 3; 1 angular direction, 2 axes in the meridional direction and 3 axes perpendicular to the element axis. In this case, the table are provided that contain the maximum value to the corresponding forces and the F11, F22 and F12 given in the graphs indicates that element force in the direction of axis 1 hoop, 2 meridional and 12 shear force that affects per unit length respectively. M11 is the moment per unit length of the element around axis 2 as shown below the (Figure).

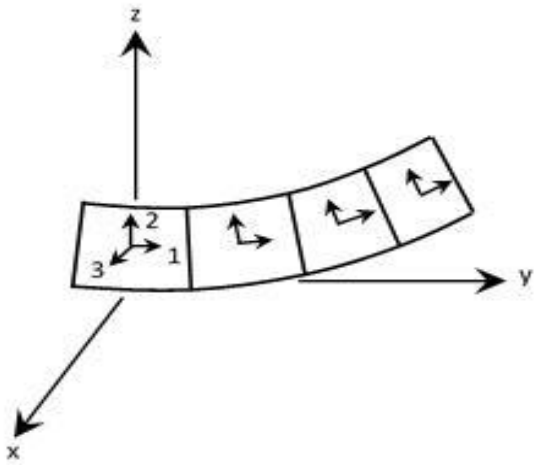

Figure 4.2 Location of the local axis set.

4.3.1 Hoop Force

Change of the hoop force along the tower height is given in Fig.4.3 and the maximum rate of change of force computed based on the table 4.2 given below. Maximum hoop forces is observed at the base of the tower like meridional force and moment. Curvature increase this force also increase along the height of the tower approximately above the throat level but below throat level behaved oppositely curvature increase force will be decreased. The maximum change between smallest and greatest curvature observed is 46.3%. When the slenderness increases, force also increased and the amount of increment is 103.91%. The other important parameter in this study is thickness effect. Hoop force decreased R/t ratio increase or thickness decrease.

This parameter does not affect at the throat level compared to cornice and slightly above base. The amount of reduction due to thickness decrement is 59.7%.

During neck level investigation maximum hoop force observed is the ratio of Z_U/Z_H=1, but for other parameters below neck level Z_U/Z_H =2, 3, 4 and 0 regularly decrease the hoop force. The maximum change observed when throat level move from the middle to peak level is 71%.

Table 4.2 Maximum hoop force

Case	d_L/d_T (curvature effect)	F11 (kN/m)	Case	H/d_T (slenderness effect)	F11 (kN/m)
1	1.75	1928.34	1	2.00	5484.54
2	2.00	1965.64	2	2.50	5557.25
3	2.25	2047.76	3	3.00	5950.73
4	2.50	2305.04	4	3.50	9640.14
5	2.75	2754.49	5	4.00	13993.89

Case	R/t (thickness effect)	F11 (kN/m)	Case	Z_U/Z_H (throat level effect)	F11 (kN/m)
1	50	7512.91	1	0	2723.00
2	75	5413.27	2	1	3376.95
3	100	3988.8	3	2	2417.32
4	125	3469.65	4	3	2653.06
5	150	2617.39	5	4	2666.29

As can be seen the plot throat level effect versus hoop force, the neck level were in the waist the force suddenly kick out because of the weakness of the tower above the neck level due to the lowering of curvature and the inverted toroid cone mass moment of inertia force direction changed to inside and the bottom part become rigged it causes the greater change in displacement results unexpected change of force magnitude.

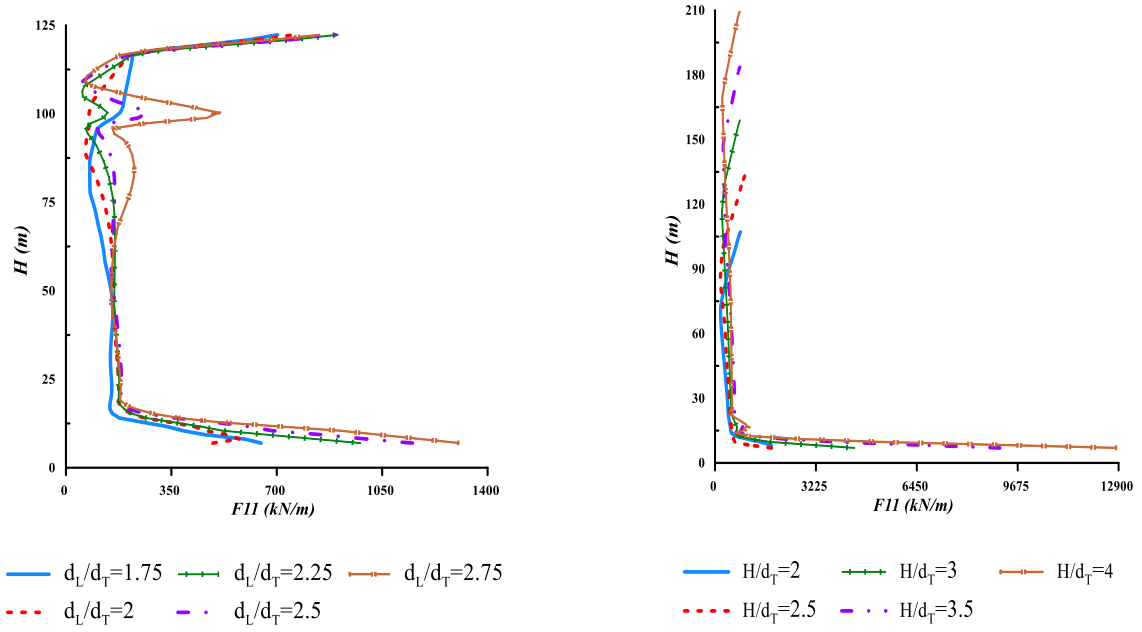

a) Curvature effect

b) Slenderness effect

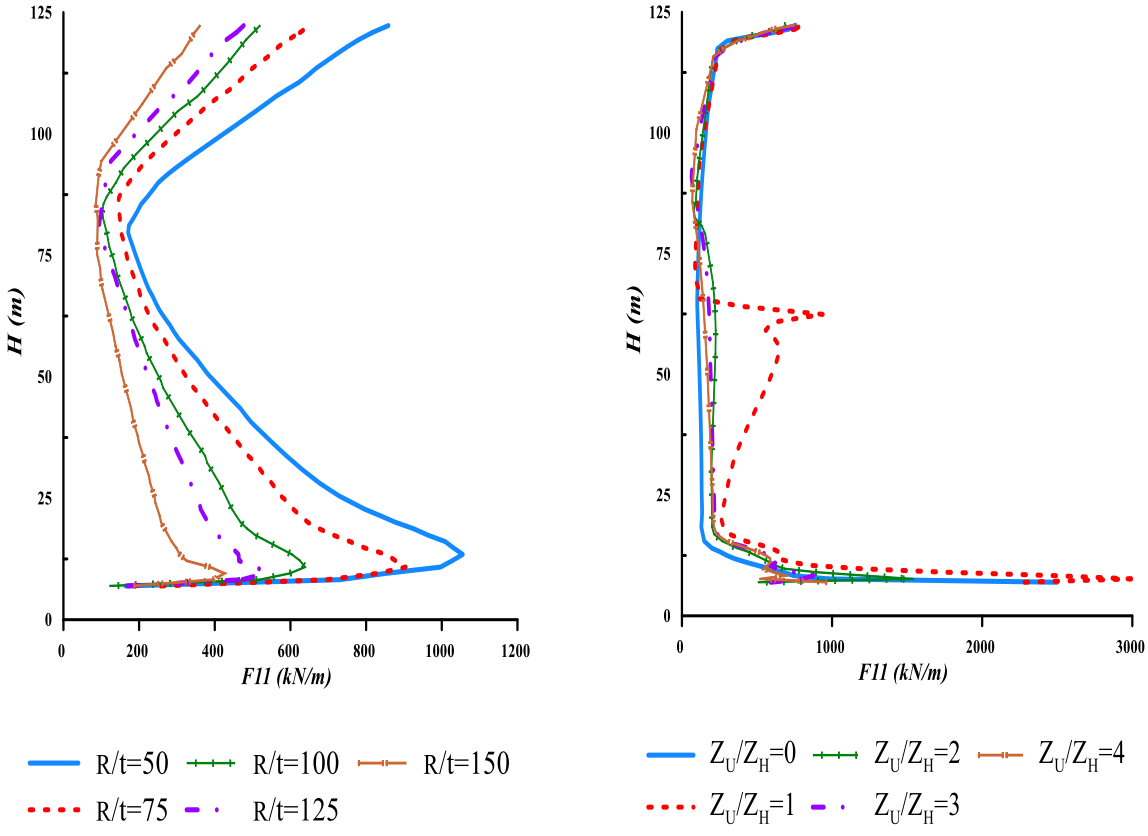

c) Thickness effect

d) Throat level effect

Figure 4.3 Change of the circumferential (hoop) forces (F11) along the height

4.3.2 Meridional Force

Change of the meridional force along the tower height is given in Fig.4.4 and its maximum value of change was computed based on table 4.3 as shown below. As the curvature increases, the meridional forces decrease to a certain height starts from the base where as when the thickness decrease the opposite behavior is true, i.e., with decreasing thickness together the meridional forces are decreasing. The biggest and the most for curvature when considering small meridional forces reduction of 24% and 71.5% for thickness change were observed. However, curvature increase the force also increased starts from approximately the middle height of the tower to peak level. As slenderness increases the meridional forces increased and also the increment of the force is around 131.5%.The other effect of throat level on meridional force at the base of the tower were governed by Z_U/Z_H=0, but along the height Z_U/Z_H=1, is more significant and contribute to higher force compared to other throat level parameter.

If the throat level gone from the middle height to zero or peak level meridional force decrease along height but it acts oppositely at the base of the tower along circumference. The maximum change observed between the smaller and greater forces became 23%. Therefore, the effect of thickness and slenderness on meridional forces are more decisive parameters.

Table 4.3 Maximum meridional force at zero degree

Case	d_L/d_T (curvature effect)	F22 (kN/m)	Case	H/d_T (slenderness effect)	F22 (kN/m)
1	1.75	3291.61	1	2.00	7743.68
2	2.00	2903.73	2	2.50	11952.38
3	2.25	2902.75	3	3.00	11617.11
4	2.50	2845.95	4	3.50	15254.2
5	2.75	2512.74	5	4.00	17910.82

Case	R/t (thickness effect)	F22 (kN/m)	Case	Z_U/Z_H (throat level effect)	F22 (kN/m)
1	50	12638.4	1	0	5097.04
2	75	7835.13	2	1	3940.96
3	100	6070.44	3	2	4415.10
4	125	4689.28	4	3	4608.56
5	150	3603.21	5	4	4507.59

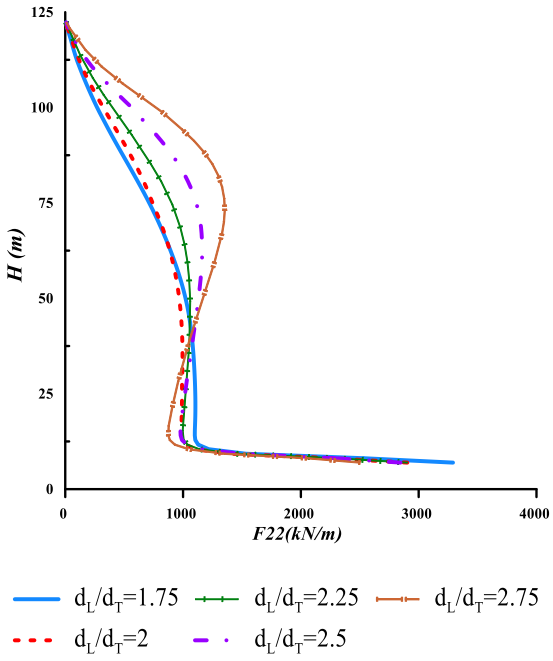

a) Curvature effect

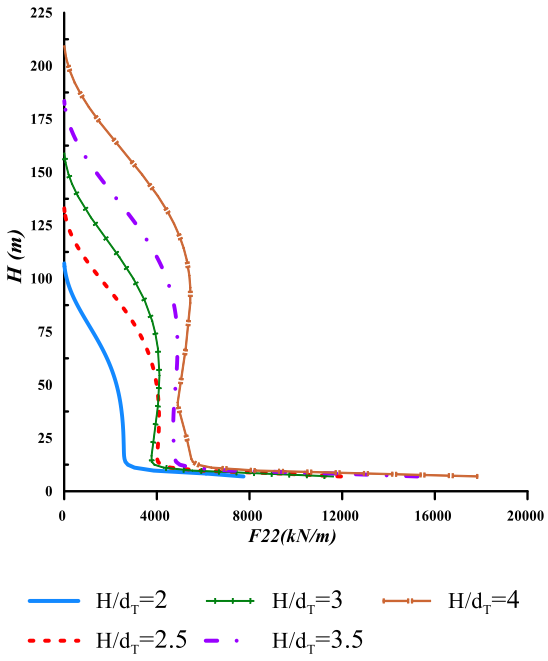

b) Slenderness effect

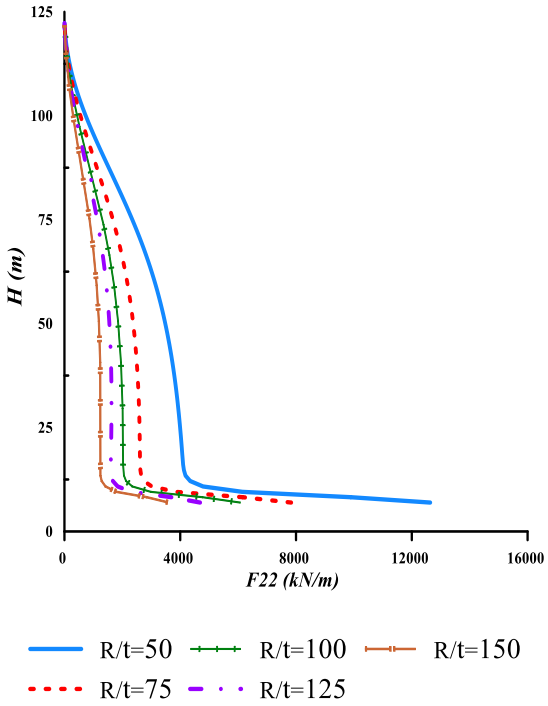

c) Thickness effect

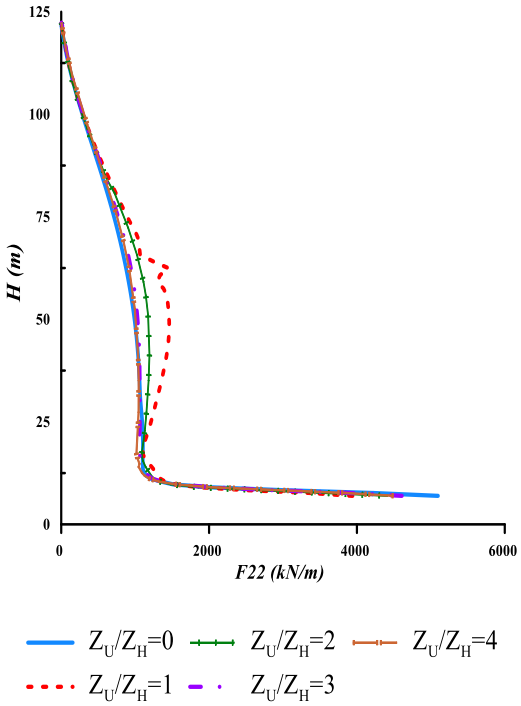

d) Throat level effect

Figure 4.4 Change of the meridional forces (F22) along the height

4.3.3 Shear Force

Maximum shear force along the height were observed slightly above the neck of the tower and the output result were recorded at 90 degree unlike other force at 0 degree. The obtained result plotted height Vs force given graphically as shown below Fig.4.5.

Curvature effect is one of the important parameters that has been studied. As we have seen, the graphical representation shear force above and below throat level has reverse properties, which means as curvature increases the shear force decreases below and increases above neck level. The observed change between maximum and minimum curvature are 43.7% and 31.0% below and above throat level respectively. As slenderness increase, shear force also increases along the height, like a curvature maximum value observed above throat level for each slenderness parameter. Due to the effect of slenderness, the amount of change between dwarf and slender cooling tower 22.0% is obtained. When the R/t ratio increases shear force along the height of the tower is decreases regularly it keeps that the maximum value also observed slightly above throat as you can see in Fig.4.5 and the change observed in the order of 67.8%. The effect of neck level another parameter that used to examine shear force along the height and circumference. The maximum values of force are represented graphically as shown in the table 4.4 below throat level, shear force increase neck level move to peak but the reverse behavior was observed above and below throat so, the maximum change observed between maximum and minimum force is 29%.

Table 4.4 Maximum meridional shear force

Case	d_L/d_T (curvature effect)	F12 (kN/m)
1	1.75	527.97
2	2.00	490.47
3	2.25	526.63
4	2.50	585.53
5	2.75	709.48

Case	H/d_T (slenderness effect)	F12 (kN/m)
1	2.00	1351.76
2	2.50	1671.02
3	3.00	1655.29
4	3.50	2047.88
5	4.00	1735.52

Case	R/t (thickness effect)	F12 (kN/m)
1	50	1831.08
2	75	1220.04
3	100	906.97
4	125	800.16
5	150	589.76

Case	Z_U/Z_H (throat level effect)	F12 (kN/m)
1	0	1527.26
2	1	1832.36
3	2	1299.71
4	3	1468.10
5	4	1558.01

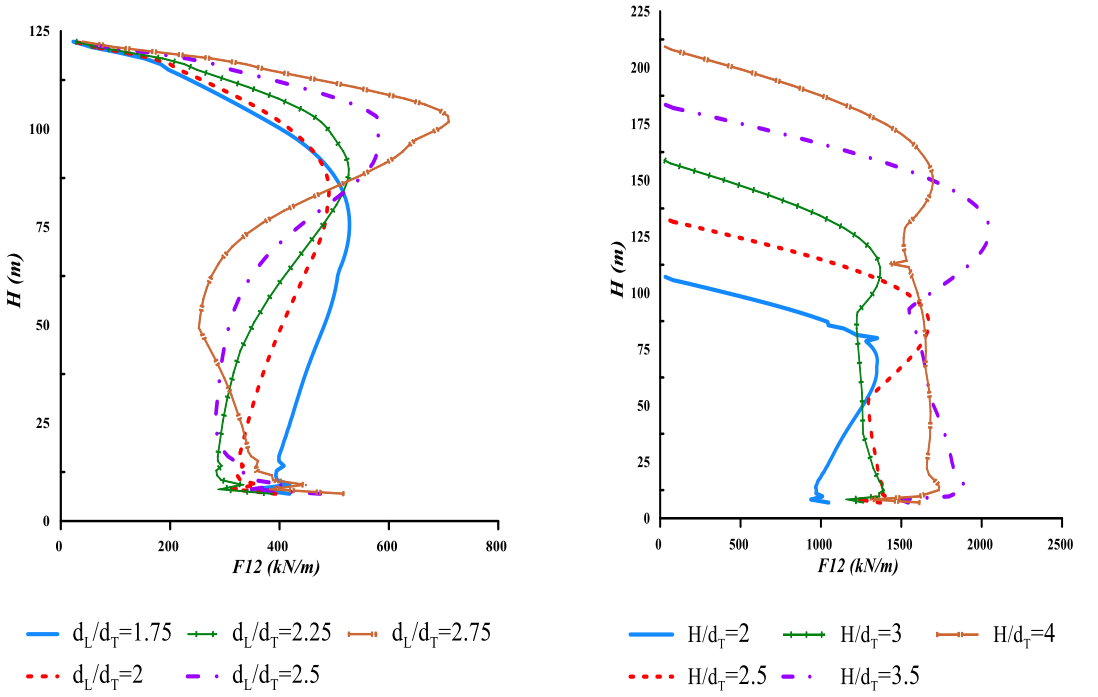

a) Curvature effect

b) Slenderness effect

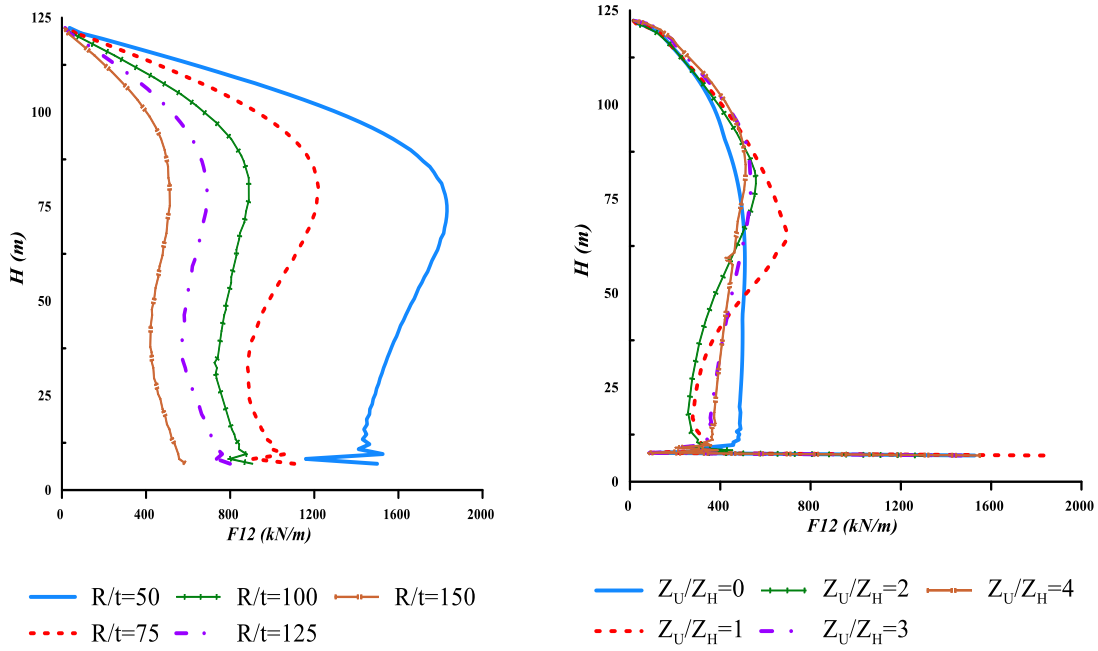

c) Thickness effect

d) Throat level effect

Figure 4.5 Change of the shear forces (F12) along the height

4.3.4 Moment

Change of the meridional moments along the tower is given in Fig.4.6. The maximum meridional moments are formed at the base of the tower as it is in the forces. Thickness decreases the meridional moments also decreased by considered the reduction in the thickness effect for the proportions was around 68.3%. The neck height is increased the meridional moment is decreased. $Z_U/ Z_H = 1$ ratio a significant change in the meridional moments and the increase in failure is due to the fact that the meridional moments. If we considered the effect of neck level, the percent of reduction will be 58.7%. Slenderness increases the moment is increased proportionally and the rate of increment were 467%. As the curvature decrease, a reduction in meridional moments was observed and the largest the reduction is about 75.8%. In the meridional moments, the effect of slenderness and curvature is more dominant and has been decisive. The largest meridional moments are presented in Table 4.5 as shown below.

Table 4.5 Maximum meridional moment at zero degree

Case	d_L/d_T (curvature effect)	M11 (kNm/m)
1	1.75	30.31
2	2.00	80.16
3	2.25	111.03
4	2.50	121.42
5	2.75	125.42

Case	H/d_T (slenderness effect)	M11 (kNm/m)
1	2.00	275.80
2	2.50	114.12
3	3.00	155.25
4	3.50	439.77
5	4.00	648.15

Case	R/t (thickness effect)	M11 (kNm/m)
1	50	243.42
2	75	180.03
3	100	127.42
4	125	103.30
5	150	77.14

Case	Z_U/Z_H (throat level effect)	M11 (kNm/m)
1	0	52.44
2	1	127.03
3	2	97.46
4	3	89.22
5	4	86.03

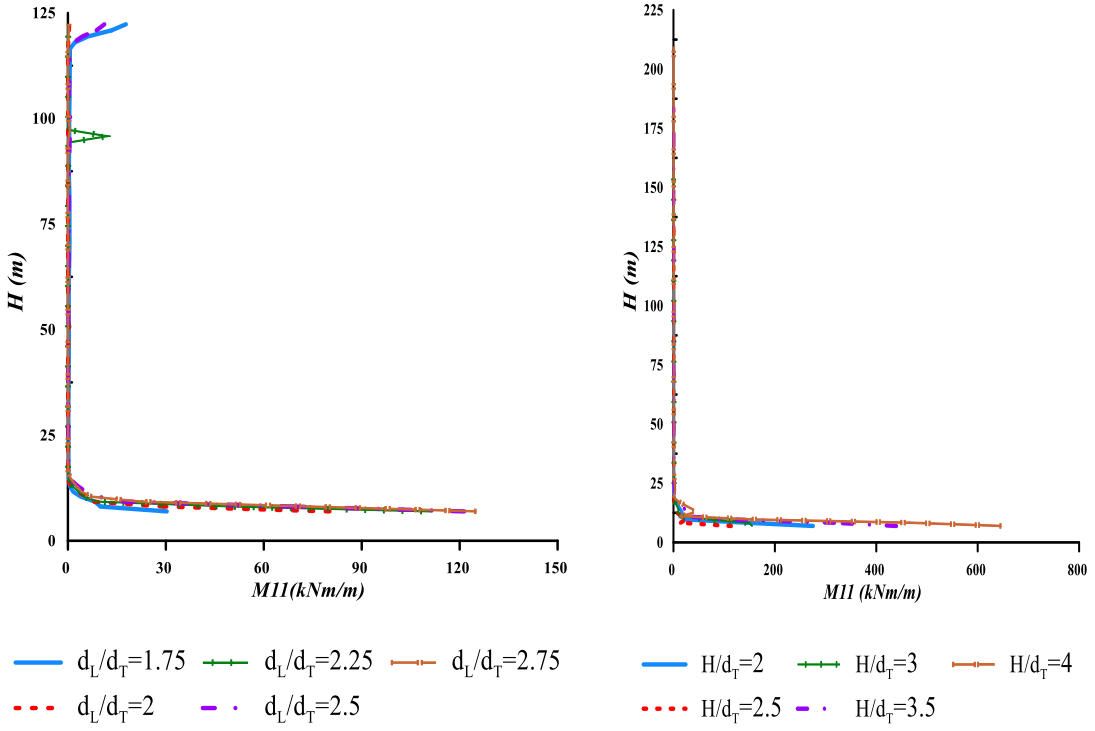

a) Curvature effect

b) Slenderness effect

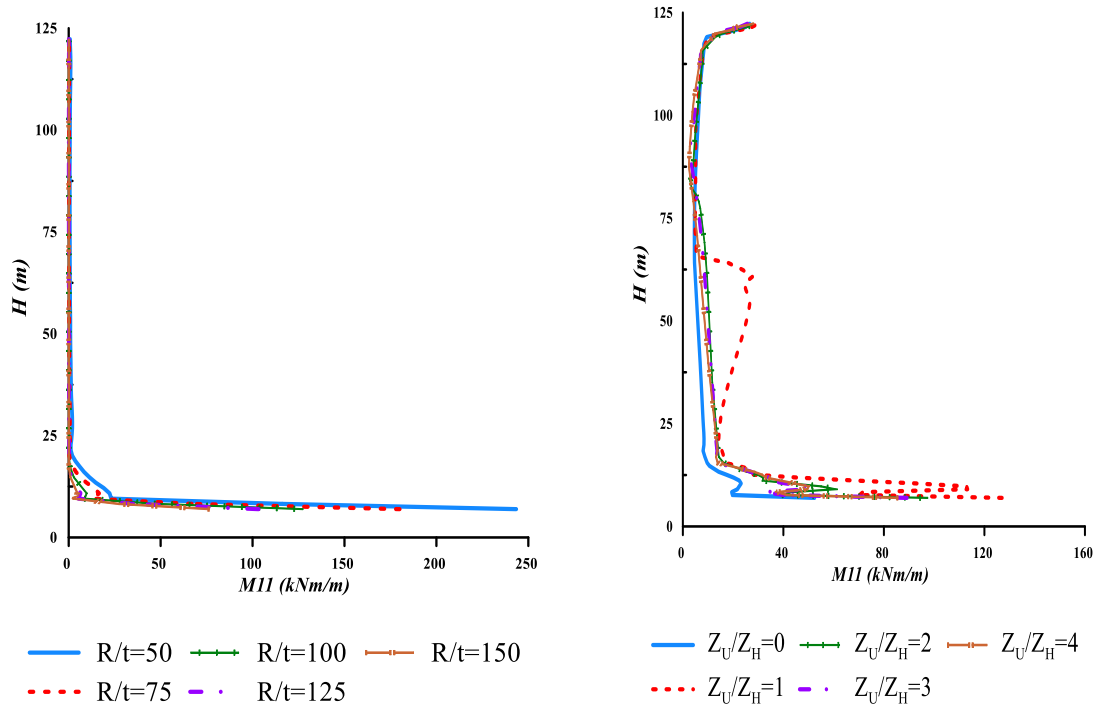

c) Thickness effect

d) Throat level effect

Figure 4.6 Change of the meridional moments along the height

4.4 Hoop, Meridional and Shear Forces around Circumference (Angular Direction)

The meridional forces obtained at the base of the tower and Angular variation of moments is given in Fig. below Tower maximum meridional force and moments at the base it has not been repeated here since it was first interpreted, as shown angular variation from 0^0 to 180^0 graphically were presented. The distribution between 180^0 and 360^0 is the same as the distribution given here. In addition, we have seen in the shapes when examining the angular changes such as the meridional forces and moments reaching large values at 0^0 and 180^0

4.4.1 Hoop, Meridional and Shear Forces at the Base of the Tower

4.4.1.1 Hoop Force

Unlike other forces and moments hoop force maximum value observed at 90^0 in angular direction and the output result presented in the Fig.4.7. Curvature increase the hoop force also increased regularly, so that the maximum rate change of hoop force due to curvature about 30% increment. The Slenderness effect more significant than other parameter and behave differently. For H/d_T=2, 2.5, 3 maximum value observed at 90 degree but for H/d_T=3.5 and 4 shifted 0 and 180 degree. Even if it is changing maximum force location the obtained rate of change were 60.8%. The effect of thickness is opposite to curvature, R/t ratio increase the hoop force will decreased and the amount of change observed between the largest and most reduced by 65.2%.

The effect of throat level on the hoop force will increased with the height of throat close to the peak except that Z_U/Z_H=0 and 1, when Z_U/Z_H=1 experience higher hoop force for the half of 180 degree and the reset is governed by Z_U/Z_H=0. The rate of change force due to the effect of throat level is 25.4%. The maximum value of hoop force obtained from analysis given in the table 4.2.

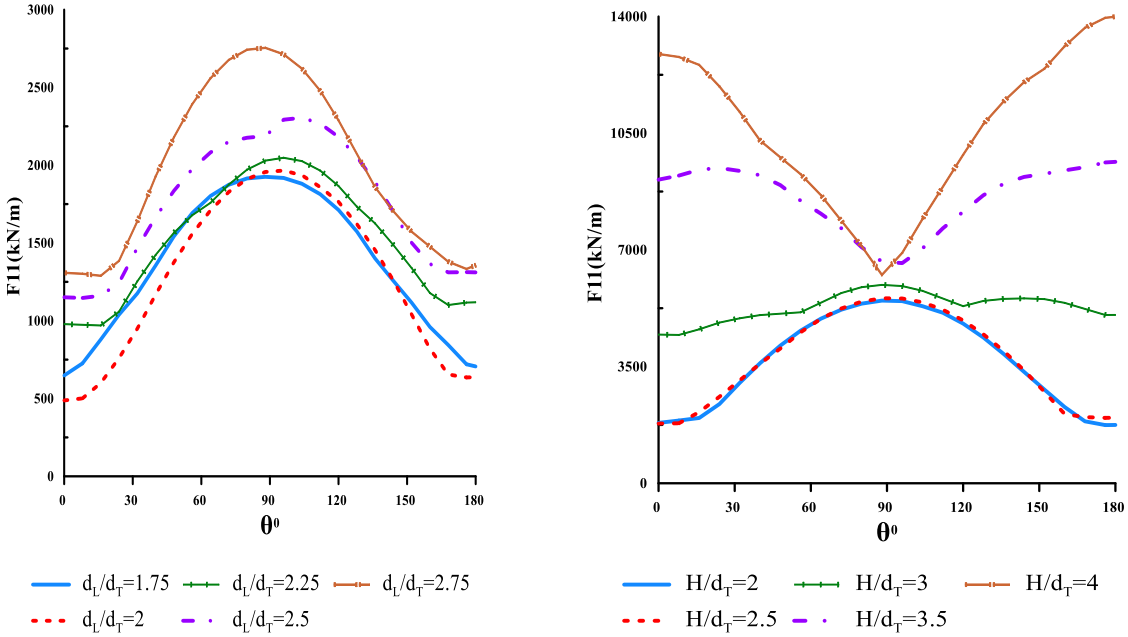

a) Curvature effect

b) Slenderness effect

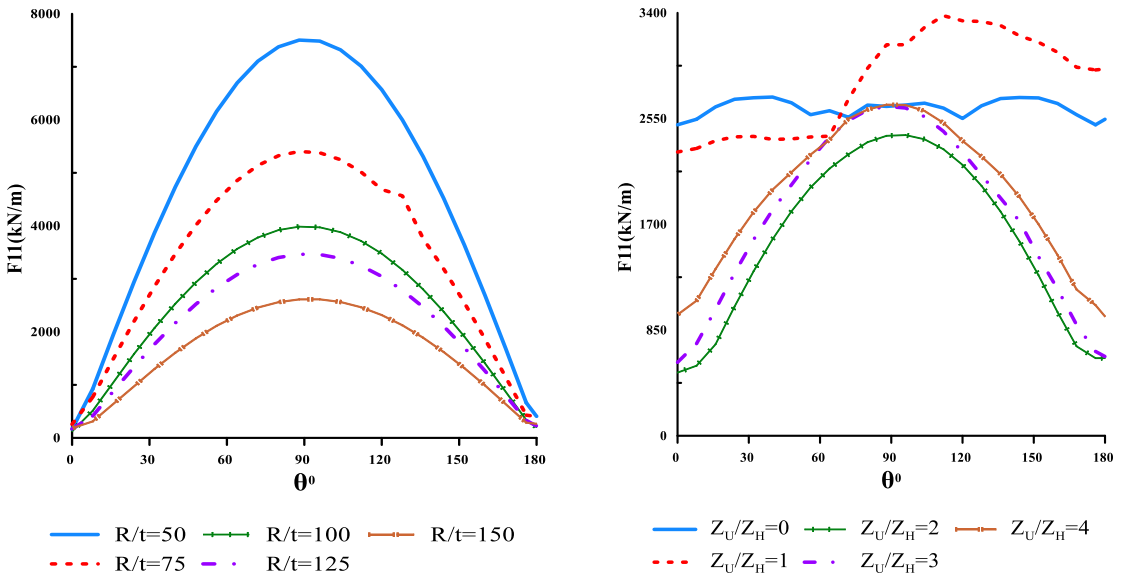

c) Thickness effect

d) Throat level effect

Figure 4.7 Angular variation of circumferential (hoop) forces at the base of the tower

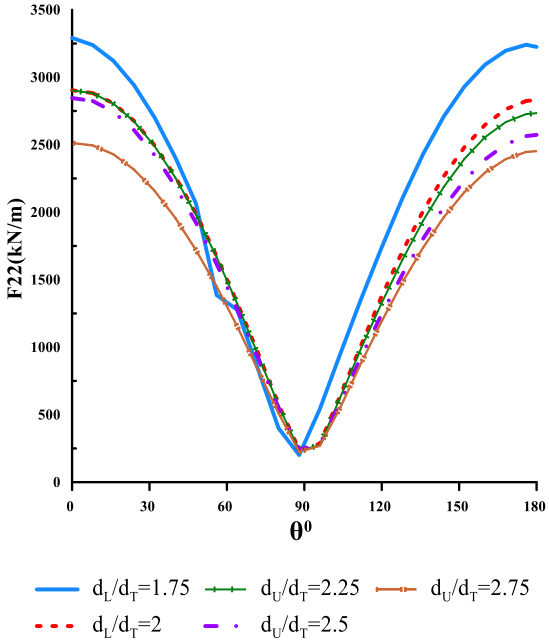

a) Curvature effect

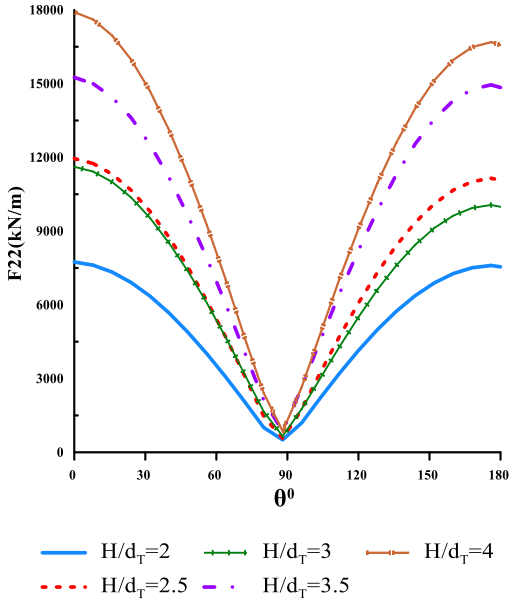

b) Slenderness effect

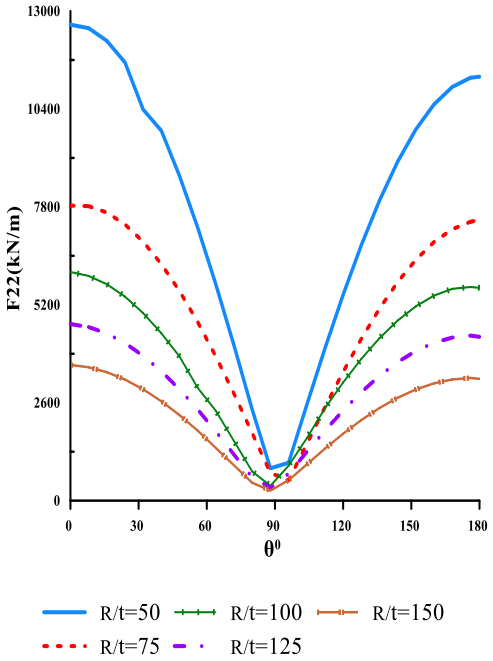

c) Thickness effect

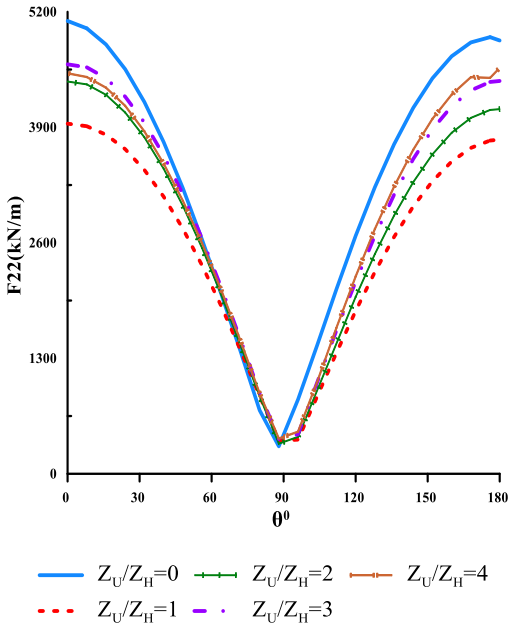

d) Throat level effect

Figure 4.8 Angular variation of meridional forces at the base of the tower

4.4.1.2 Shear Force

The shear forces obtained at the base level in angular direction is given in Fig.4.10. As the Curvature increase, the shear and meridional force at the base of the tower will be decreased regularly and its effect opposite to shear force. The maximum reduction of the force was observed by the increment of curvature about 25.6% of change and the slenderness increase shear force proportionally increased by the rate of change 52.9%. The R/t ratio increase or thickness decrease the shear force also decreased by 67.7%. For the throat level ratio Z_U/Z_H =2, 3 and 4 shear force increase respectively. However, in the case of Z_U/Z_H =1 (neck level at middle) and 0 (neck level at peak) approximately share similar character but the higher shear force will be observed at Z_U/Z_H =0 or at the base of the tower. The rate of change between maximum and minimum shear force due to the effect of neck level is 14.8%. the maximum value obtained from analysis presented below the table 4.6.

Table 4.6 Maximum shear force at the base

Case	d_L/d_T (curvature effect)	F12 (kN/m)
1	1.75	1145.07
2	2.00	1004.51
3	2.25	1004.18
4	2.50	927.37
5	2.75	849.97

Case	H/d_T (slenderness effect)	F12 (kN/m)
1	2.00	2622.02
2	2.50	4004.75
3	3.00	3655.29
4	3.50	5105.02
5	4.00	5563.2

Case	R/t (thickness effect)	F12 (kN/m)
1	50	3843.24
2	75	2602.28
3	100	2038.17
4	125	1626.94
5	150	1239.65

Case	Z_U/Z_H (throat level effect)	F12 (kN/m)
1	0	1527.26
2	1	1832.36
3	2	1301.14
4	3	1468.10
5	4	1558.01

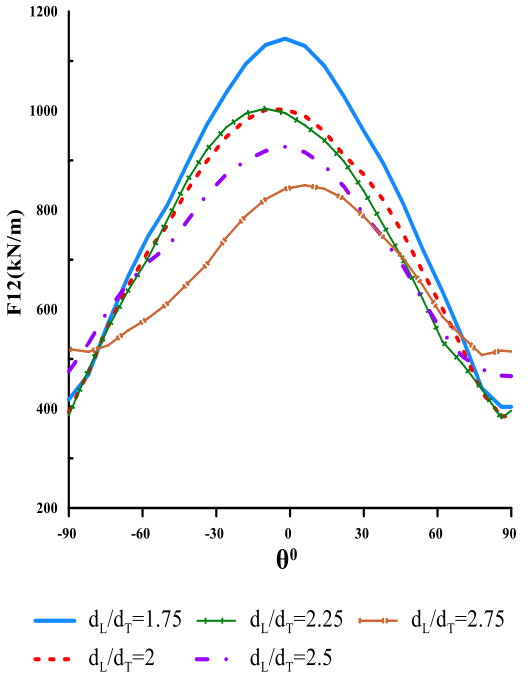

a) Curvature effect

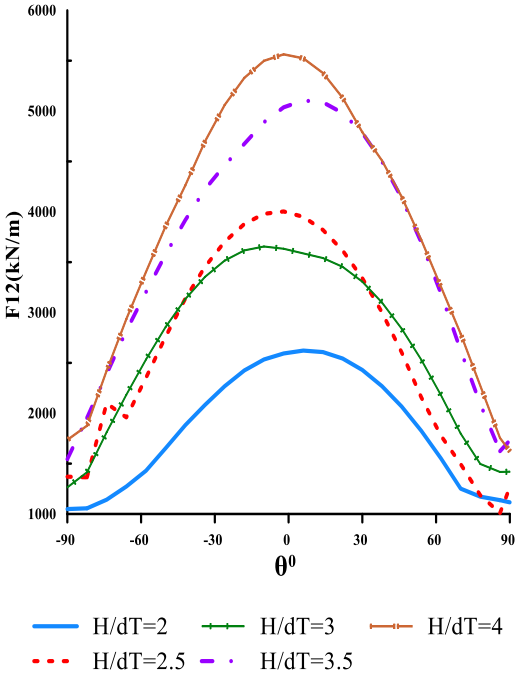

b) Slenderness effect

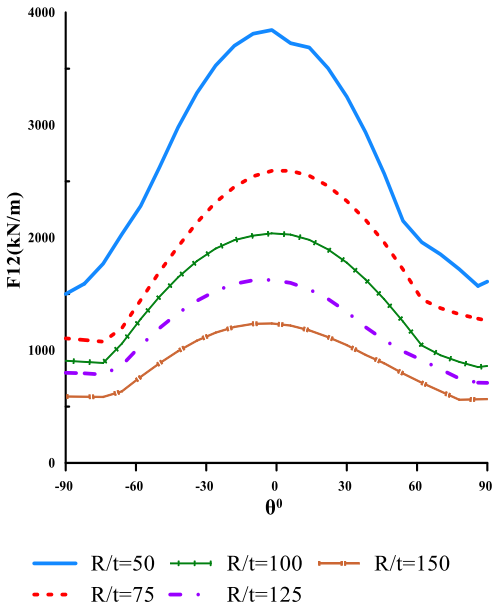

c) Thickness effect

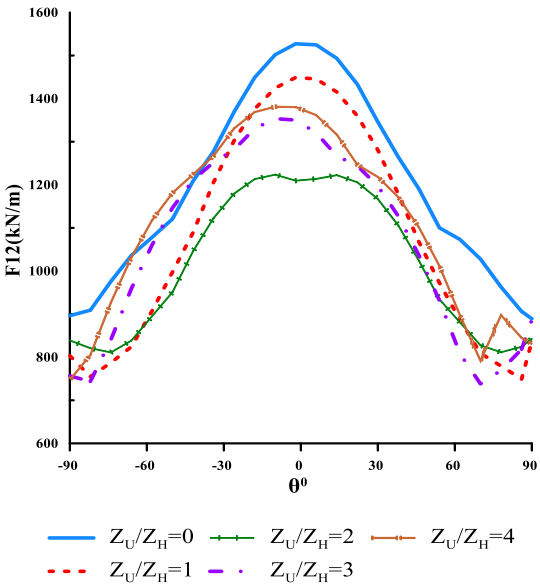

d) Throat level effect

Figure 4.9 Angular variation of shear forces at the base of the tower

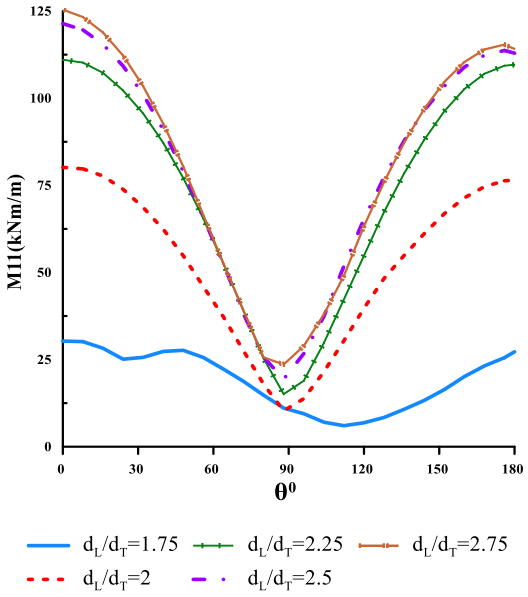

a) Curvature effect

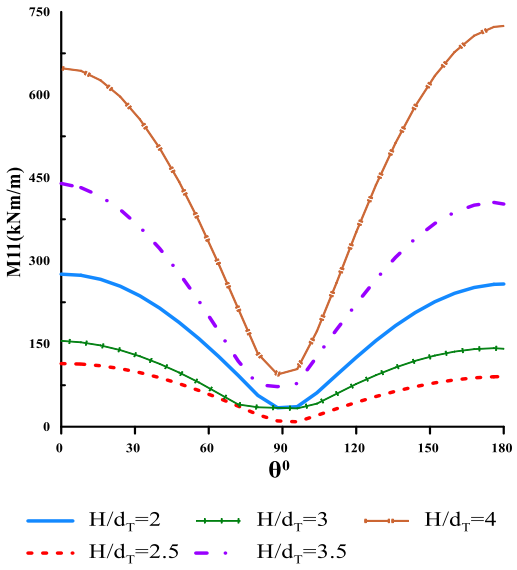

b) Slenderness effect

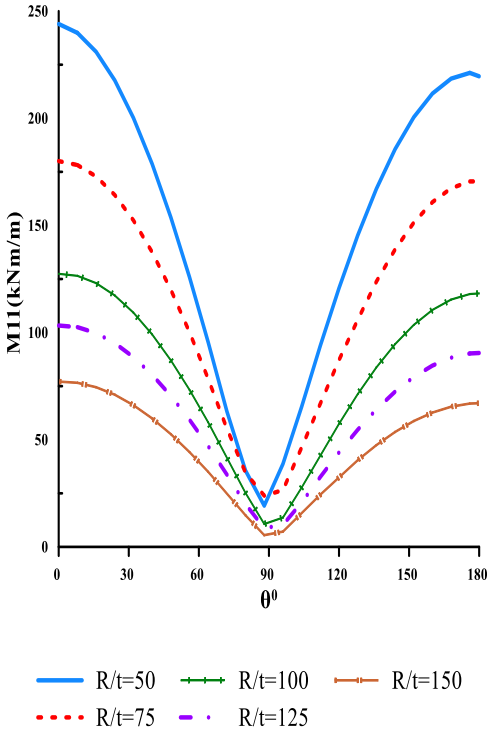

c) Thickness effect

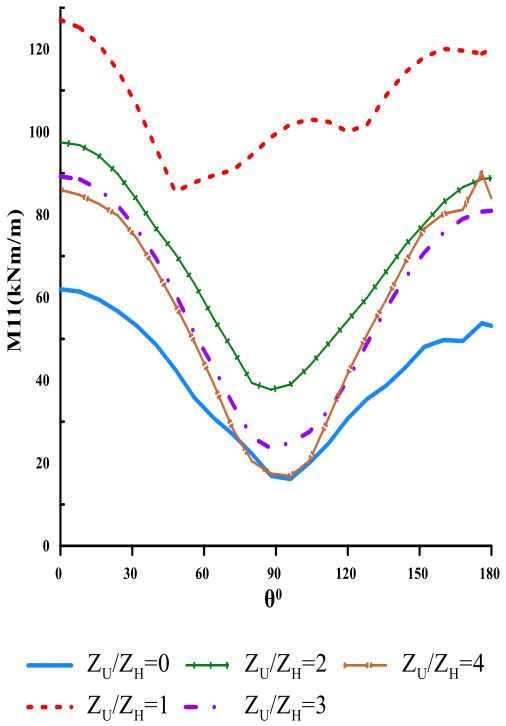

d) Throat level effect

Figure 4.10 Angular variation of meridional moment at the base of the tower

4.4.2 Meridional and Shear Forces at the Neck Level of the Tower

4.4.2.1 Shear Force

The shear forces obtained at the neck level in angular direction is given in Fig.4.11. As you can see from the figures, shear forces increased at neck level as curvature increases. Between the largest and smallest shear forces, the amount of increase is about 51.4%. Thickness effect on the shear forces, thickness decrease this force also decreased at the neck level and the greatest reduction by the amount of 63.7%. As neck height increases, the shear forces at the neck level are decreased. Here too the reduction rate is about 97.8%. As slenderness increases, the shear forces in the neck level increased and the greatest change is 65.6%. Eventually, shear at the neck level for variables it can be said that there are significant changes in forces. Obtained the largest shear forces as shown in Table 4.7 is presented.

Table 4.7 Maximum shear force at the neck

Case	d_L/d_T (curvature effect)	F12 (kN/m)
1	1.75	443.40
2	2.00	466.34
3	2.25	555.82
4	2.50	581.19
5	2.75	671.26

Case	H/d_T (slenderness effect)	F12 (kN/m)
1	2.00	1043.25
2	2.50	1431.13
3	3.00	1388.04
4	3.50	1727.74
5	4.00	1667.96

Case	R/t (thickness effect)	F12 (kN/m)
1	50	1357.35
2	75	960.85
3	100	748.73
4	125	638.21
5	150	492.05

Case	Z_U/Z_H (throat level effect)	F12 (kN/m)
1	0	15.44
2	1	688.59
3	2	611.03
4	3	539.39
5	4	464.76

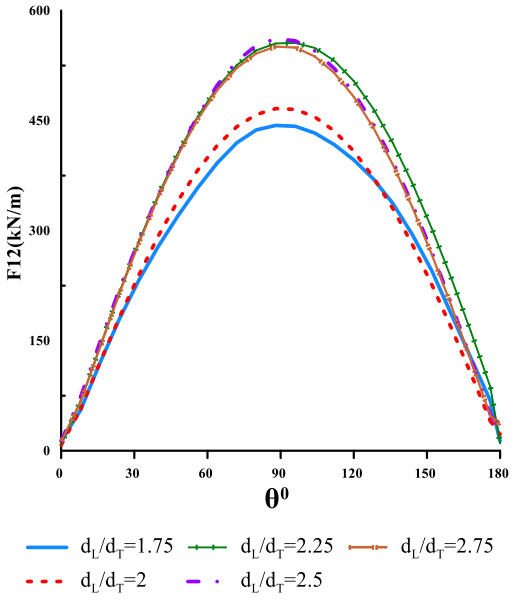

a) Curvature effect

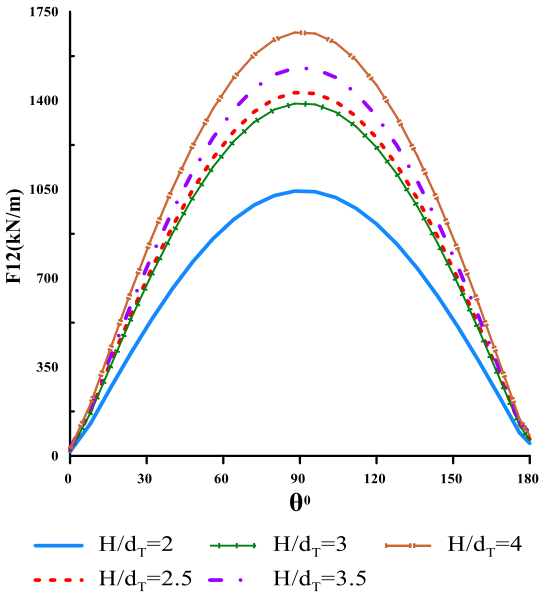

b) Slenderness effect

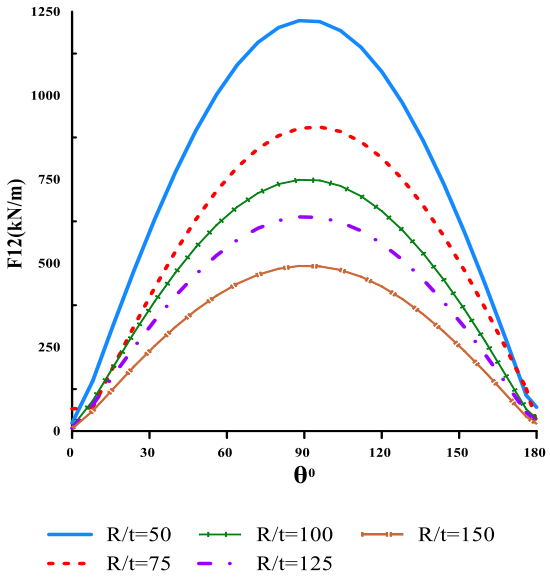

c) Thickness effect

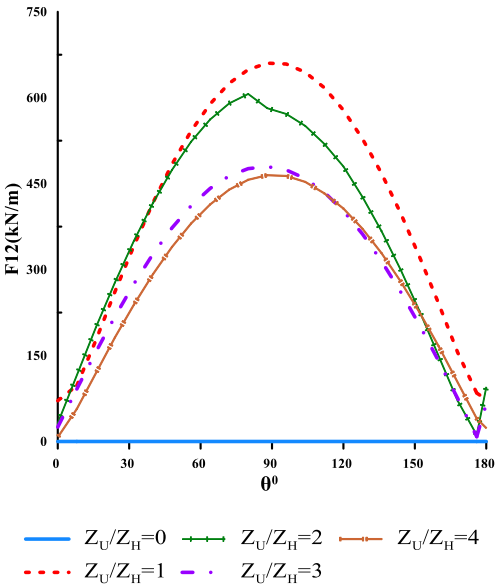

d) Throat level effect

Figure 4.11 Angular variation of circumferential (hoop) forces at neck level

4.4.2.2 Meridional force

The meridional forces obtained at the neck level in angular direction is given in Fig.4.12. As you can see from the figures meridional forces increased at neck level as curvature increases. Between the largest and smallest meridional forces, the amount of increase is about 184%. Thickness effect on the meridional forces, thickness decrease meridional force also decreased at the neck level and the greatest reduction by the amount of 59.8%. As neck height increases, the meridional forces at the neck level are decreased. Here too the reduction rate is about 99.8%. As slenderness increases, the meridional forces in the neck level increased and the biggest change is 214.6%. Eventually, meridional at the neck level for variables it can be said that there are significant changes in forces. Obtained the largest meridional forces are shown in Table 4.8 is presented.

Table 4.8 Maximum meridional force at the neck

Case	d_L/d_T (curvature effect)	F22 (kN/m)	Case	H/d_T (slenderness effect)	F22 (kN/m)
1	1.75	289.83	1	2.00	589.45
2	2.00	361.42	2	2.50	959.26
3	2.25	518.82	3	3.00	1156.24
4	2.50	600.83	4	3.50	1600.11
5	2.75	822.29	5	4.00	1854.36

Case	R/t (thickness effect)	F22 (kN/m)	Case	Z_U/Z_H (throat level effect)	F22 (kN/m)
1	50	803.20	1	0	2.84
2	75	603.73	2	1	1386.47
3	100	471.82	3	2	669.50
4	125	420.60	4	3	475.87
5	150	323.22	5	4	340.78

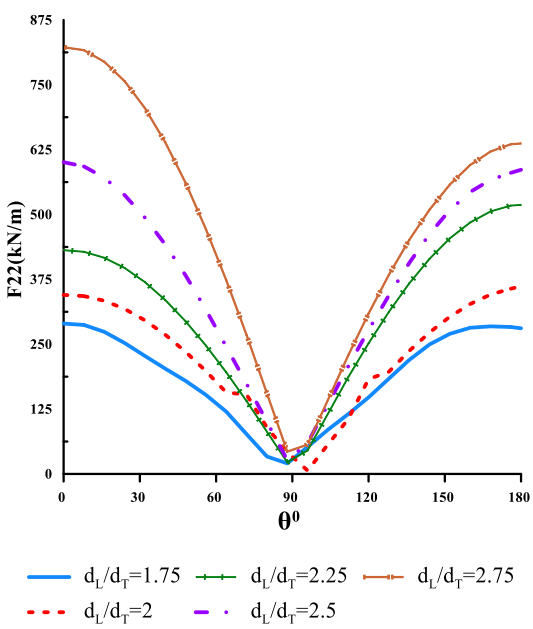

a) Curvature effect

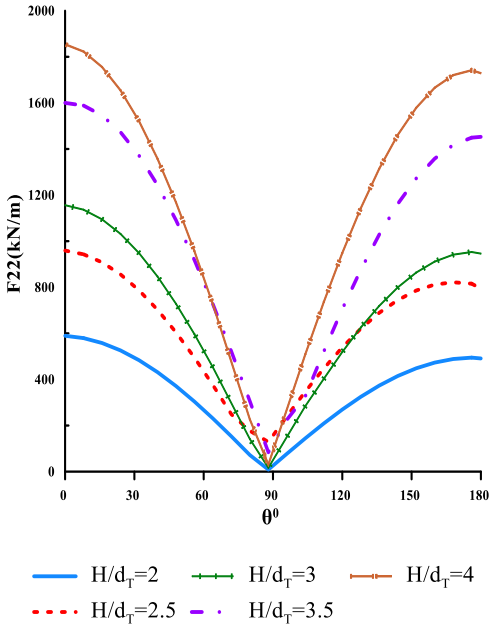

b) Slenderness effect

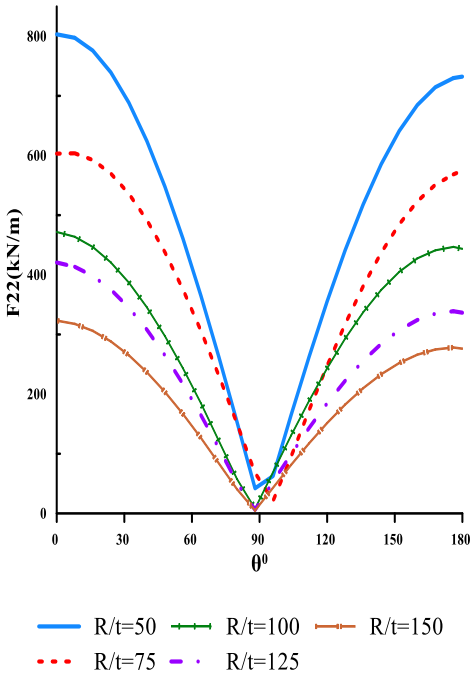

c) Thickness effect

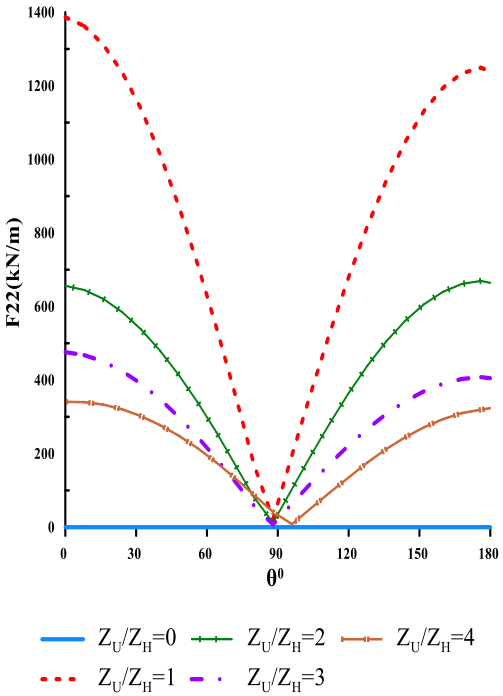

d) Throat level effect

Figure 4.12 Angular variation of meridional forces at neck level

4.4.3 Meridional Forces at the Peak Level of the Tower

Change meridional force at angular direction are given Fig.4.13. As shown in the figure, the curvature increases meridional forces are also increasing at peak level. The greatest increase by the change of 81.8%. As the thickness decreases, the meridional forces at the peak level are also reduced and the biggest the reduction is 61.5%. Slenderness and neck level are changed, the meridional forces obtained at the top of the tower also changed. At the top, thickness and curvature effects are more dominant and decisive parameter on meridional forces. The most obtained major meridional forces are presented in Table 4.9

Table 4.9 Maximum meridional force at the peak

Case	d_L/d_T (curvature effect)	F22 (kN/m)
1	1.75	5.98
2	2.00	5.43
3	2.25	6.92
4	2.50	9.87
5	2.75	9.63

Case	H/d_T (slenderness effect)	F22 (kN/m)
1	2.00	4.58
2	2.50	5.23
3	3.00	4.80
4	3.50	5.60
5	4.00	5.26

Case	R/t (thickness effect)	F22 (kN/m)
1	50	5.30
2	75	3.97
3	100	2.97
4	125	2.66
5	150	2.04

Case	Z_U/Z_H (throat level effect)	F22 (kN/m)
1	0	2.84
2	1	3.15
3	2	3.12
4	3	3.33
5	4	3.05

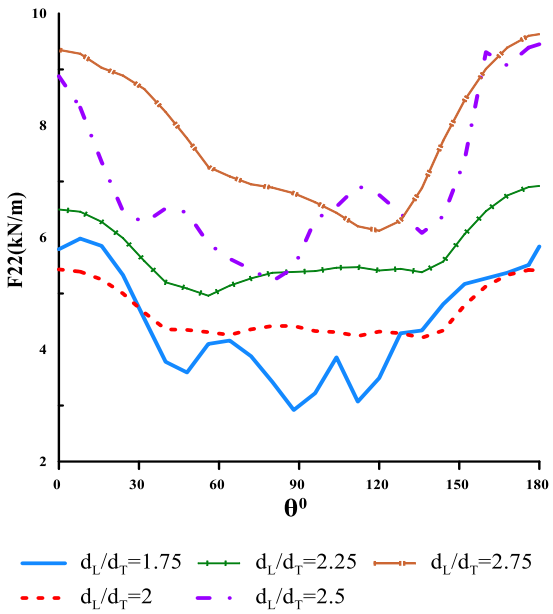

a) Curvature effect

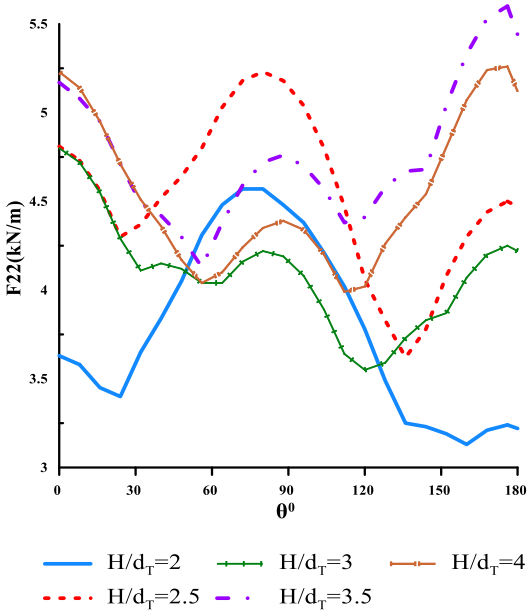

b) Slenderness effect

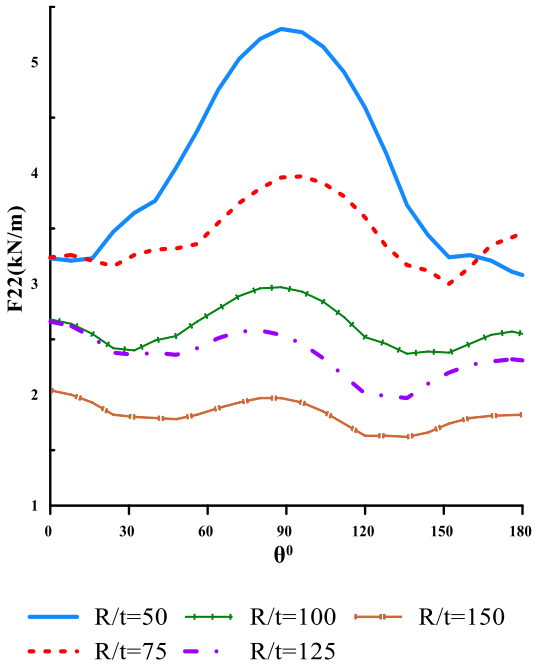

c) Thickness effect

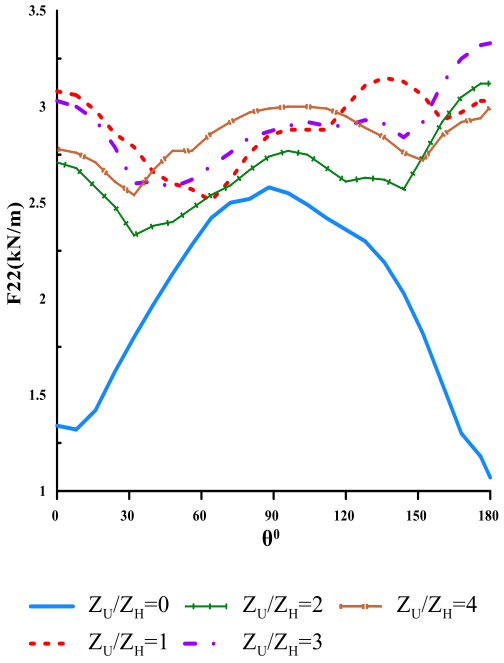

d) Throat level effect

Figure 4.13 Angular variation of the meridional forces at the peak level

CHAPTER 5 CONCLUSION AND RECOMMENDATION

5.1 Conclusion

A trace of the studies that have been performed on cooling towers in general has been presented. The studies literature have been divided into numerical and experimental/field studies. The literature review tables of these studies in a chronologically dated. The cooling tower's geometrical parameters were changed in a systematic manner in order to obtain the relationship between the dynamic characteristics and shape of the cooling tower's geometrical parameters. Ratios of the cooling tower's dimensions were considered to cover a wider geometrical spectrum.

Hyperbolic cooling towers are large and delicate structures. Therefore, it is great importance for designers to know their dynamic behaviors. This study was presented for the purpose of before I have mentioned by changing the geometry of the tower a parametric work has been carried out. The slenderness, the curvature, the crust thickness and height of neck level effects on dynamic behavior was investigated. All the parameters are considered behavior of hyperbolic cooling towers under earthquake is changed. This conclusion drawn by categorizing in to two subsection.

5.1.1 Displacement, Force and Moment along Height

- When looking at horizontal displacement of the tower height, the effect of slenderness and acceptance of thickness it is more dominant and determinant than other parameter.

- Hoop and shear force increase with curvature above neck level (confirmed investigation bay Nasir et.al 2002) and decrease below while meridional force decrease with curvature around base of tower and increase starts from slightly above base under dynamic ground accelerations.

- Slenderness and thickness increase with hoop, shear and meridional force increases. When we consider the effect of throat level, the throat level move from middle height to peak level hoop and meridional force decrease while shear force increase.

- Neck level, slenderness and thickness more dominant factor for hoop, meridional and shear force respectively. This information will require the establishment of a curvature to limit these forces to desirable levels even other parameter dominate because most of the designer assuming that the problem of stability minimized by increasing curvature in seismic design.

- Curvature, thickness increase and neck level close to peak moment decrease while slenderness increase moment also increase. Curvature and slenderness more significant effect and require careful selection of height and curvature under seismic design.

5.1.2 Force at Base, Neck and Peak Level of the Tower in Angular Direction

- Hoop force increase with curvature, slenderness and neck level increases and decreases where the thickness decrease under consideration of hoop force thickness is the dominant factor at the base of the tower.

- Shear and meridional force decrease when curvature increase. However, slenderness and thickness increase with the force and share similar characteristic with neck level effect except that $Z_U/Z_H=0$ (look conical shape) and 1(above waist look cylinder). During the selection of neck level should be careful and advised to select in between two cases.

- However, thickness and slenderness on the meridional force and moment has more effect at the base while neck level and thickness is more than other parameter at neck level. Where curvature and slenderness increase shear and meridional force also increase at neck level but the reverse is true for the case of throat level and thickness.

- At peak level thickness and curvature has the dominant effect on meridional force.

- As a result, the displacements and forces are changed with the geometry so it should be kept between the desired limit values. Therefore, both economic and safe design can be achieved by taking into account many parameters

5.2 Recommendation

The following recommendation are made in light of the research findings that have been graphically represented previously in chapter four.

- A set of design guideline can be developed for conceptual design of hyperbolic natural draft cooling tower by systematic creation of chart that represent displacements, forces and moment behavior when compared to wide range of geometrical parameters presented in this study.

- Hyperbolic cooling towers subjected to seismic loading are more sensitive to the change in geometry. Therefore, more attention should be paid by the analyst on the modeling of the tower.

- Since the seismic response was limited to linear analysis of hyperbolic cooling tower, further studies should be done to create model that optimize the shape of tower supported by experiment.

REFERENCES

1. Asadzadeh, E. & Alam, M., 2014. A survey on hyperbolic cooling towers. International journal of civil, structural, construction and architectural engineering, 8(10), pp. 1027-1039.
2. Asadzadeh, E., Alam, M. & Asadzadeh , S., 2014. Dynamic response of layered hyperbolic cooling tower considering the effects of support inclinations. Structural engineering and mechanics, 50(6), pp. 797-816.
3. Baillis, C., Jullien, J. & Limam, A., 2000. An enriched 2D modelling of cooling towers. Effects of real damage on the stability under self weight and on the strength under wind pressure. Engineering structures, Volume 22, pp. 831-845.
4. Bamu, P. & Zingoni, A., 2005. Damge, deterioration and the long-term structural performance of cooling-tower shells: A survey of developments over the last 50 years. Engineering structures, Volume 27, pp. 1794-1799.
5. Bhimaraddi, A., Moss, P. & Carr, A., 1991. Free-vibration response of column-supported, ring-stiffened cooling tower.Journal of engineering mechanics, 117(4), pp. 770-788.
6. Busch, D., Reinhard, H., Kratzih, W. & Montag, U., 2002. New natural draft cooling tower of 200m of height. Engineering structures, Volume 24, pp. 1509-1521.
7. Choi, C.-K. & Noh, H.-C., 2000. Stochastic analysis of shape imperfection in rc cooling tower shells. Journal of structural engineering, 126(3), pp. 417-423.
8. Gould, P. & Kratzig, W., 1999. Cooling tower structures. Chen Wai-Fah Boca Raton: CRCC Press LLC.
9. Gould, P., Ravichandran, R. & Sridharan, S., 1998. A local-global FE model for non-linear analysis of column- supported shells of revolution. Thin-walled structures, Volume 31, pp. 25-37.
10. Hara, T., 2015. Dynamic response property of cooling tower structures. Challenge journal of structural mechanics, 1(1), pp. 38-41.
11. Jang, H. & Min, C., 2001. Design and inelastic behaviour of hyperbolic cooling towers. KSCE Journal of civil engineering, 5(4), pp. 309-318.
12. Jia, X., 2013. Revisiting the failure mode of a RC hyperbolic cooling tower, considering changes of material and geometric properties. Engineering structures, Volume 47, pp. 148-153.

13. Julian, A., Dumitrescu, A., Croll , J. & Billington , D., 1983. Cooling towers on flexible foundations. Journal of structural engineering , 109(10), pp. 2248-2264.
14. Kaiser, T., Elwi, A. & Mioduchowski, A., 1995. Nonlinear harmonic analysis applied to axisymmetric structures. Computers and structures, Volume 55, pp. 1107-1118.
15. Kim, J., Lee, J. & Yoon, H., 2015. Free vibration analysis for shells of revolution based on p-version mixed finite element formulation. Finite elements in analysis and design, Volume 95, pp. 12-19.
16. Kopenetz, L. & Catarig, A., 2011. Practically structural analysis of large cooling towers. Journal of applied engineering sciences, 1(14-4), pp. 39-44.
17. Kulkarni, S. & Kulkarni, A., 2014. Static and dynamic analysis of hyperbolic cooling tower. Journal of civil engineering technology and research, 2(1), pp. 39-61.
18. Lang, C., Meiswinkel, R. & Filippou, F., 2002. No-linear analysis of shells of revolution with ring elements. Engineering structures, Volume 24, pp. 163-176.
19. Lang, C. & Straus, J., n.d. Natural draft cooling tower design and construction in Germany - Past (since 1965), present and future. s.l.:s.n.
20. Lin, F. et al., 2014. Prediction of ground motion due to the collapse of a large-scale cooling tower under strong earthquakes. Soil dynamics and earthquakes engineering, Volume 65, pp. 43-53.
21. Li, Y., Lin, F., Gu, X. & Lu, X., 2014. Numerical research of a super-large cooling tower subjected to accidental loads. Nuclear engineering and design, Volume 269, pp. 184-192.
22. Long-yuan, L. & Wen-da, L., 1987. Nonlinear buckling analysis of hyperbolic cooling tower shell with ring-stiffeners. Applied mathematics and mechanics, 10(2), pp. 113-118.
23. Mahmoud, B. & Gupta, A., 1995. Inelastic large displacement behavior and buckling of cooling towers. Journal of structural engineering, 121(6), pp. 961-965.
24. Meschke, G., Mang, H. & Kosza, P., 1991. Finite element analysis of cracked cooling tower shell. Journal of structural engineering, 117(9), pp. 2620-2639.
25. Nasir, A., Thambiratnam, D., Butler, D. & Austin, P., 2002. Dynamics of axisymmetric hyperbolic shell structures. Thin-walled structures, Volume 40, pp. 665-690.

26. Noh, H., 2006. Non-linear behaviour and ultimate load bearing capacity of reinforced concrete natural draught cooling tower shell. Engieering structures, Volume 28, pp. 399-409.
27. Noorzaei, J. et al., 2006. Non-linear interactive analysis of cooling tower-foundation-soil interaction under unsymmetrical wind load. Thin-walled structures, Volume 44, pp. 997-1004.
28. Norton, R. & Weingarten, V., n.d. The effect of asymmetric imperfections on the earthquake response of hyperbolic cooling towers. Unpublished.
29. Prabhakar, N., 1990. Structural design aspects of hyperbolic cooling towers. Technical Session IV. Paper No. 9, National seminar on cooling towers: 18-20.
30. Sabhouri-Ghomi, S. & Kharrazi, M., 2005. Reinforced concrete column-supported hyperboloid cooling tower stability assessment for seismic loads. Scientia Iranica, 12(2), pp. 241-246.
31. Sabhouri-Ghomi, S., Kharrazi, M. & Javidan, P., 2006. Effect of stiffening rings on buckling stability of RC hyperbolic cooling towers. Thin-walled structures, Volume 44, pp. 152-158.
32. Sabhouri-Ghomi, S., Nik, F., Roufegarinejad, A. & Bradford, M., 2006. Numerical study of the nonlinear dynamic behaviour of reinforced concrete cooling towers under earthquake excitation. Advances in structural engineering, 9(3), pp. 1-9.
33. Sahana, L. & Sulaiman, S., 2013. The effect of seismic and wind loads on cooling tower of varying RCC shell thickness and size of shell opening. International journal of emerging trends in engineering and development, 4(3), pp.248-259.
34. Shu, W. & Wen-da, L., 1990. Theoretical and experimental solutions of cooling-tower-soil system. Journal of engineering mechanics, 116(4), pp. 862-869.
35. Tomas, A. & Tovar, J., 2012. The influence of initial geometric imperfections on the buckling load of single and double curvature concrete shells. Computers and structures, Volume 96-97, pp. 34-45.
36. Veena, N., Sulaiman, S. & Aswath, M., 2013. Comparative study of the effect of seismic and wind loads on cooling tower with A-Frame and H-Frame column supports. International journal of science and technology, 1(2), pp. 23-32.
37. Viladkar, M., Godbole, P. & Krishna, P., 1997. Finite element analysis of column supported hyperbolic cooling towers using semi-loof shell and beam elements. Engineering structures, Volume 20, pp. 75-84.

38. Viladkar, M., Karisiddappa, Bhargava, P. & Godbole, P., 2006. Static soil-structure interaction response of hyperbolic cooling towers to symmetrical wind loads. Engineering structures, Volume 28, pp. 1236-1250.
39. Yang, T., Gran, C. & Lo, H., n.d. Theoretical study of earthquake response of a cooling tower. Unpublished.

APPENDIX A

Geometric Parameter and Software Modeling of Cooling Tower Shell

Table A 1 Parameter for study

Parameter	Ratio	Height above throat (Z_H)	Height below throat (Z_U)	Total height (H)	Top diameter ($d_{C)}$	Throat diameter (d_T)	Base diameter (d_L)
Curvature	d_L/d_T=1.75	24.090	91.260	122.300	27.535	27.595	48.291
	d_L/d_T=2	24.090	91.260	122.300	27.535	24.461	48.291
	d_L/d_T=2.25	24.090	91.260	122.300	27.535	21.463	48.291
	d_L/d_T=2.5	24.090	91.260	122.300	27.535	19.317	48.291
	d_L/d_T=2.75	24.090	91.260	122.300	27.535	17.56	48.291
Slendemess	H/d_T=2	20.243	80.973	107.216	27.535	25.304	48.291
	H/d_T=2.5	25.304	101.216	132.52	27.535	25.304	48.291
	H/d_T=23	30.365	121.459	157.824	27.535	25.304	48.291
	H/d_T=3.5	35.426	141.702	183.128	27.535	25.304	48.291
	H/d_T=4	40.846	161.946	208.792	27.535	25.304	48.291
Thickness	R/t=50	24.090	91.260	122.300	27.535	25.304	48.291
	R/t=75	24.090	91.260	122.300	27.535	25.304	48.291
	R/t=100	24.090	91.260	122.300	27.535	25.304	48.291
	R/t=125	24.090	91.260	122.300	27.535	25.304	48.291
	R/t=150	24.090	91.260	122.300	27.535	25.304	48.291
Neck level	Z_U/Z_H=0	0.000	115.350	122.300	27.535	25.304	48.291
	Z_U/Z_H=1	57.650	57.650	122.300	27.535	25.304	48.291
	Z_U/Z_H=2	38.450	76.690	122.300	27.535	25.304	48.291
	Z_U/Z_H=3	28.838	86.513	122.300	27.535	25.304	48.291
	Z_U/Z_H=4	23.070	92.280	122.300	27.535	25.304	48.291

Table A 2 Example of cooling tower Geometric data

Geometric Parameter			
Total Height (m)	107.216	Height below Throat (m)	80.973
Throat Diameter (m)	25.304	Top Thickness (mm)	500
Base Diameter (m)	48.291	Throat thickness (mm)	170
Height above Throat (m)	20.243	Base Thickness (mm)	700
Geometric Ratio			
Height/Throat Diameter	2	Thickness (m)	0.5
FEM Node	**Cooling Tower Radius (m)**	**Similar to X**	**Cooling Tower Height (m)**	**Shell curvature (m)**
Node	X	Y	Z	b
1	48.291	0	80.973	49.815
2	47.753	0	79.728	49.815
3	47.214	0	78.473	49.815
4	46.674	0	77.210	49.815
5	46.132	0	75.939	49.815
6	45.590	0	74.659	49.815
7	45.047	0	73.370	49.815
8	44.504	0	72.074	49.815
9	43.961	0	70.769	49.815
10	43.417	0	69.457	49.815
11	42.874	0	68.137	49.815
12	42.332	0	66.810	49.815
13	41.790	0	65.475	49.815
14	41.250	0	64.134	49.815
15	40.711	0	62.785	49.815
16	40.174	0	61.429	49.815
17	39.639	0	60.066	49.815
18	39.106	0	58.697	49.815
19	38.576	0	57.322	49.815
20	38.049	0	55.941	49.815
21	37.525	0	54.553	49.815
22	37.006	0	53.159	49.815
23	36.490	0	51.760	49.815
24	35.980	0	50.355	49.815
25	35.474	0	48.945	49.815
26	34.974	0	47.530	49.815
27	34.480	0	46.109	49.815
28	33.992	0	44.684	49.815
29	33.511	0	43.254	49.815
30	33.038	0	41.819	49.815

31	32.573	0	40.380	49.815
32	32.117	0	38.937	49.815
33	31.669	0	37.490	49.815
34	31.231	0	36.039	49.815
35	30.804	0	34.584	49.815
36	30.388	0	33.126	49.815
37	29.983	0	31.664	49.815
38	29.591	0	30.199	49.815
39	29.211	0	28.731	49.815
40	28.845	0	27.261	49.815
41	28.493	0	25.787	49.815
42	28.157	0	24.311	49.815
43	27.835	0	22.833	49.815
44	27.531	0	21.353	49.815
45	27.243	0	19.871	49.815
46	26.973	0	18.387	49.815
47	26.721	0	16.901	49.815
48	26.488	0	15.414	49.815
49	26.274	0	13.926	49.815
50	26.081	0	12.437	49.815
51	25.908	0	10.947	49.815
52	25.756	0	9.456	49.815
53	25.625	0	7.964	49.815
54	25.517	0	6.472	49.815
55	25.430	0	4.980	49.815
56	25.366	0	3.488	49.815
57	25.324	0	1.996	49.815
58	25.305	0	0.505	49.815
59	25.310	0	-0.986	47.178
60	25.339	0	-2.477	47.178
61	25.393	0	-3.966	47.178
62	25.473	0	-5.455	47.178
63	25.576	0	-6.942	47.178
64	25.705	0	-8.428	47.178
65	25.856	0	-9.912	47.178
66	26.032	0	-11.395	47.178
67	26.229	0	-12.875	47.178
68	26.449	0	-14.354	47.178
69	26.690	0	-15.830	47.178
70	26.952	0	-17.304	47.178
71	27.234	0	-18.775	47.178
72	27.535	0	-20.243	47.178

An example of one cooling tower's geometrical parameters and meridional profile is shown in the Figure below. The figure shows the cooling tower's height, diameters, throat height to total height ratio and height to throat diameter ratios. In addition, the figure shows the variation of the cooling tower's radius with height as well as the variation of the curvature of the meridian with height. The node number, radius and height obtained in the manner shown in the Figure below were copied into the software model in order to obtain the profile of the meridian for each cooling tower that was analyzed for the parametric study.

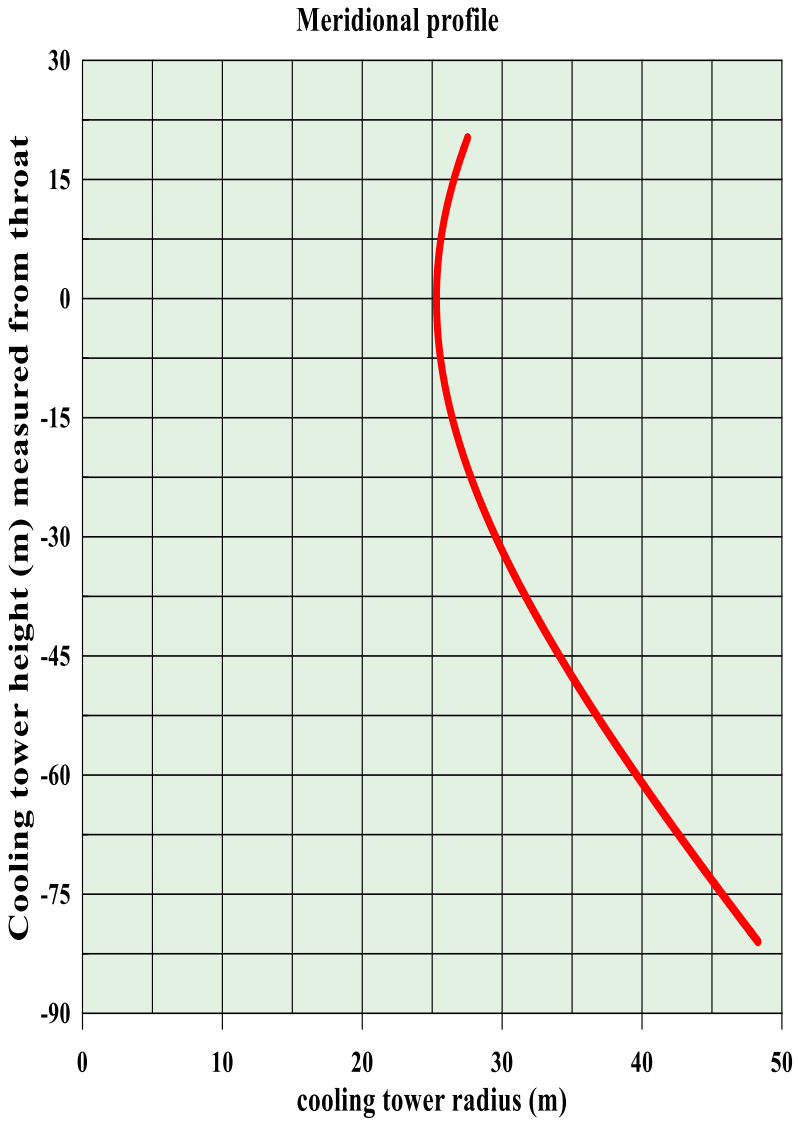

Figure A 1 Meridional profile

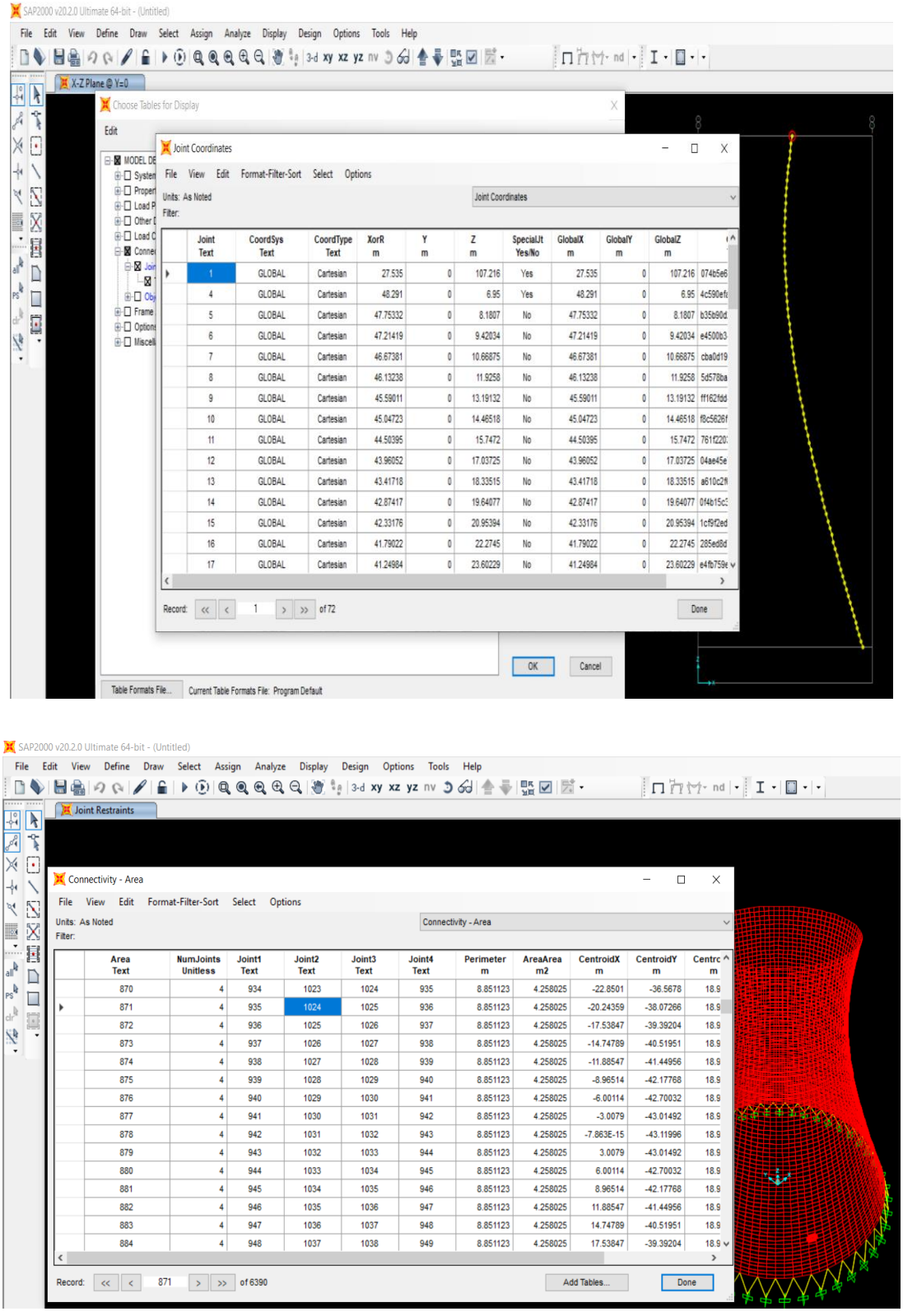

Figure A 2 Software modeling of cooling Tower shell

APPENDIX B

Graph of displacement and force along height and circumference

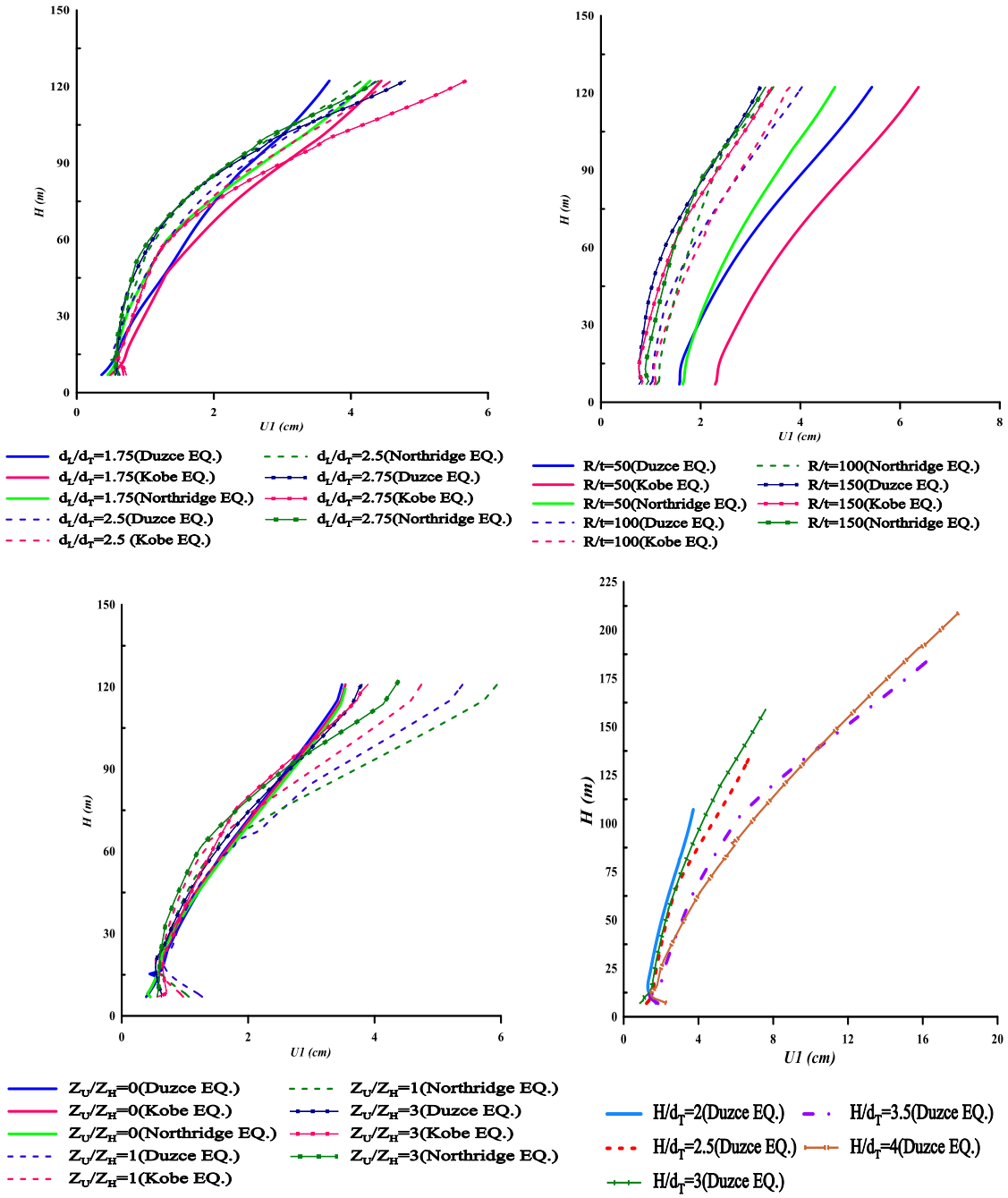

Figure B 1 Displacement for curvature, thickness, and neck level and slenderness effect respectively left to right

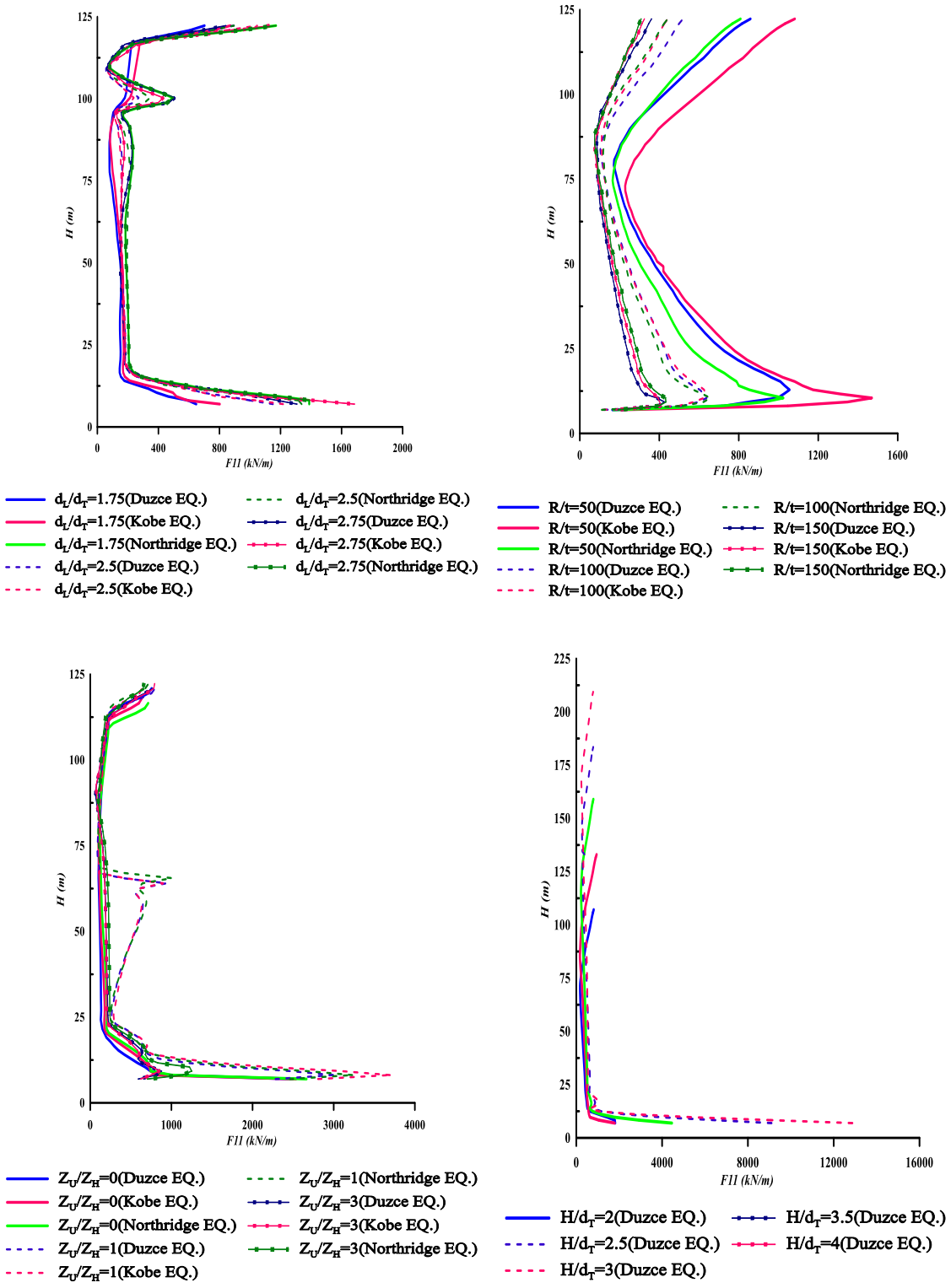

Figure B 2 Hoop force for curvature, thickness, and neck level and slenderness effect respectively left to right

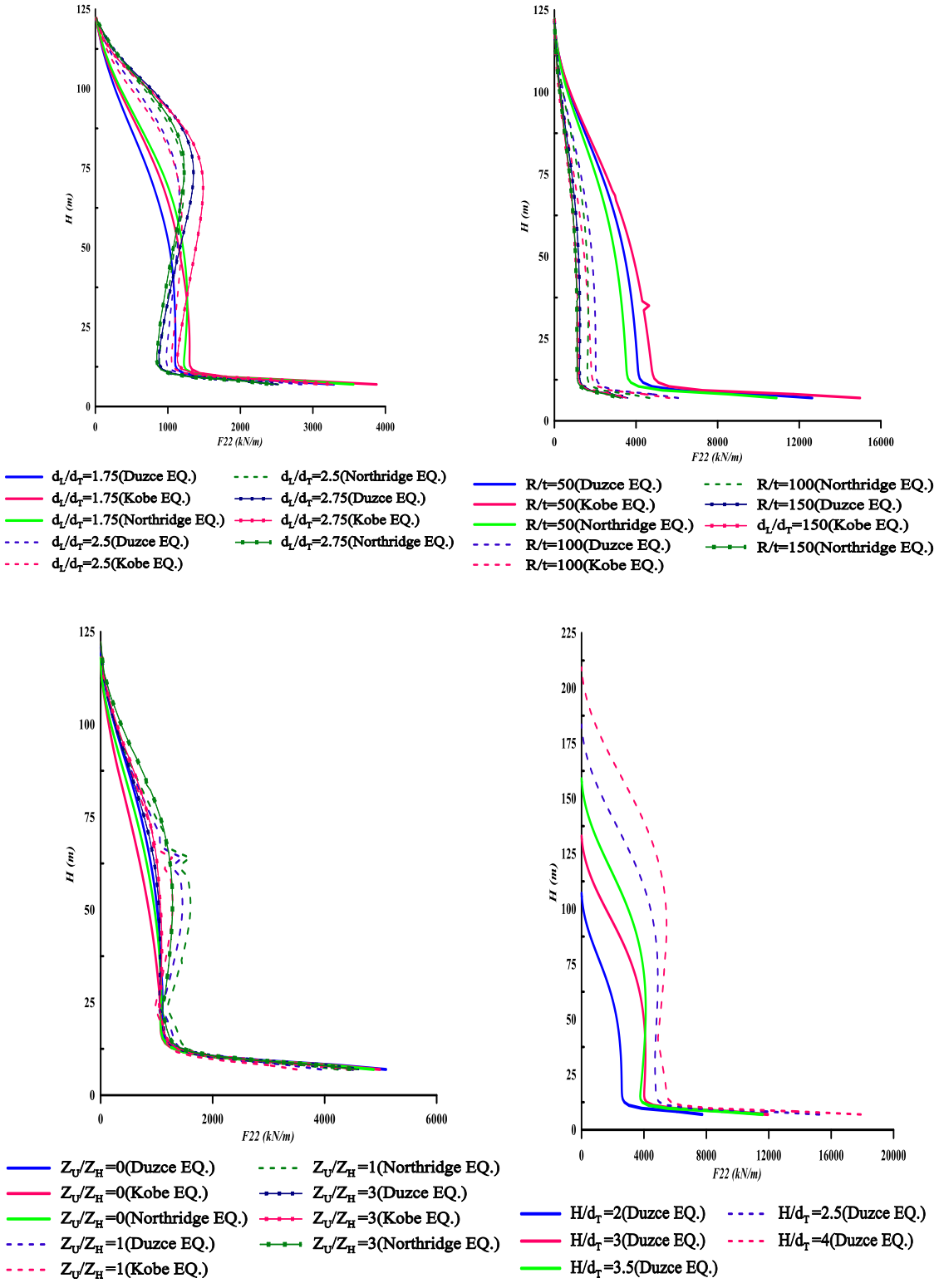

Figure B 3 Meridional force for curvature, thickness, and neck level and slenderness effect respectively left to right

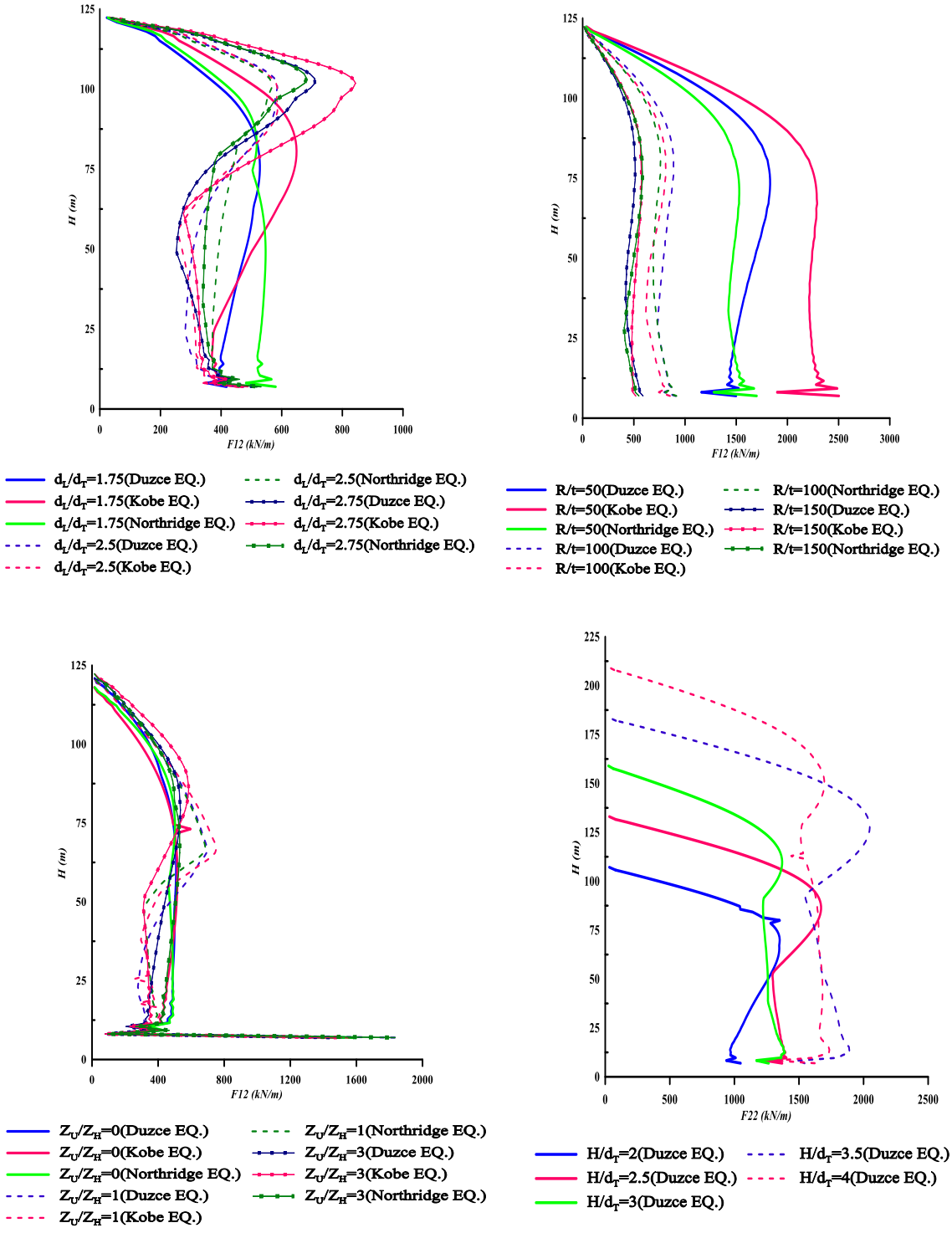

Figure B 4 Shear force for curvature, thickness, and neck level and slenderness effect respectively left to right

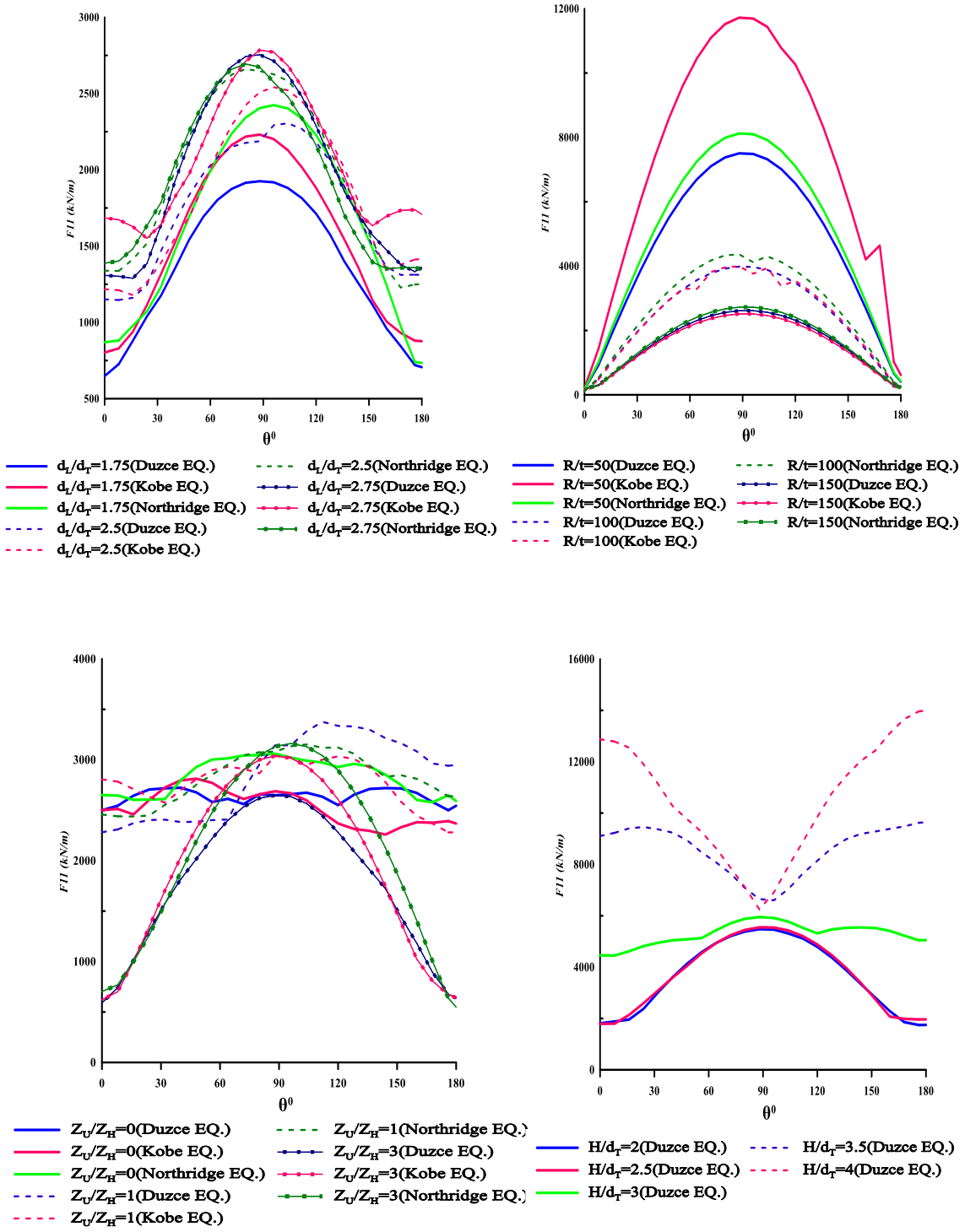

Figure B 5 Hoop force for curvature, thickness, and neck level and slenderness effect respectively left to right

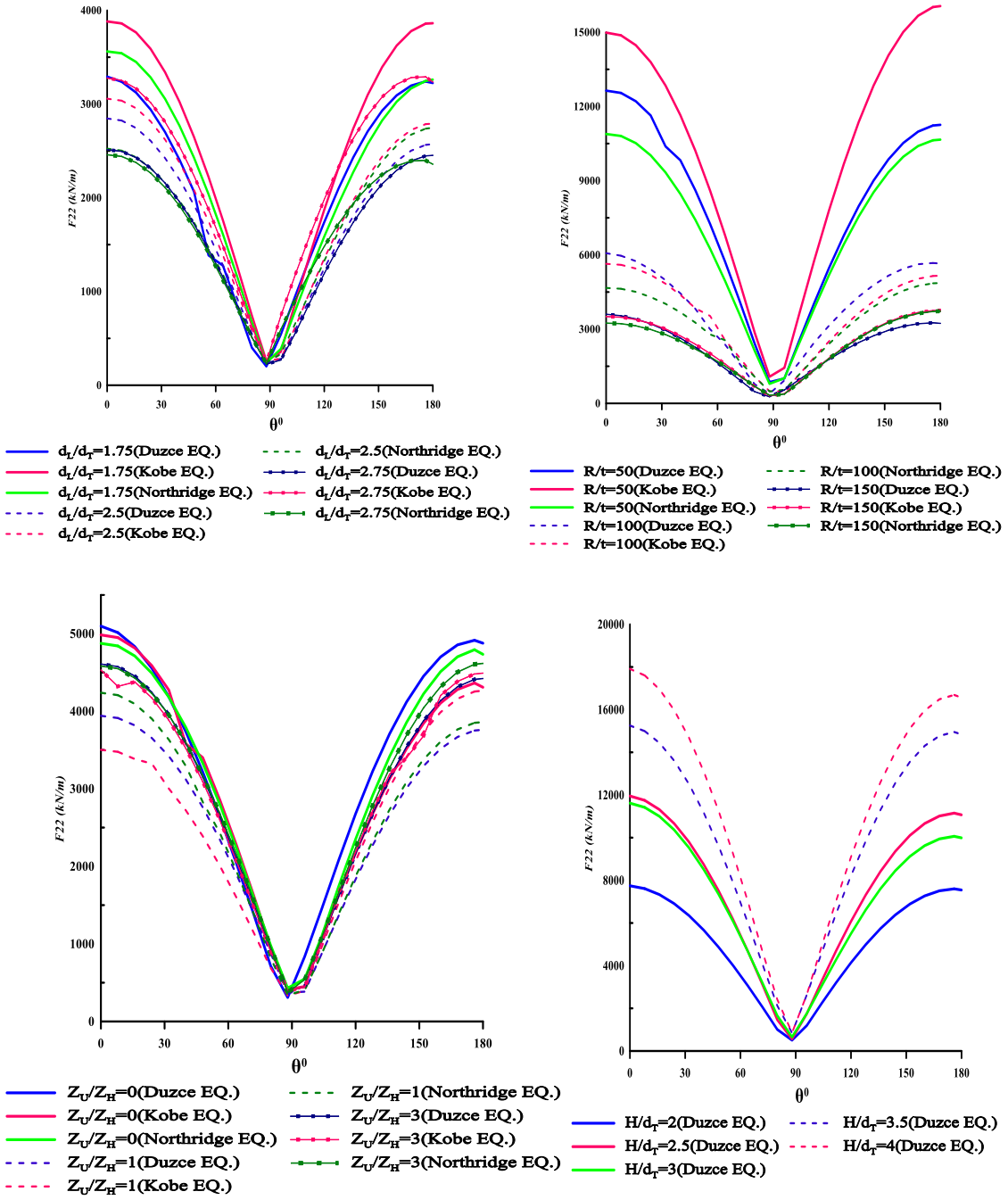

Figure B 6 Meridional force for curvature, thickness, and neck level and slenderness effect respectively left to right

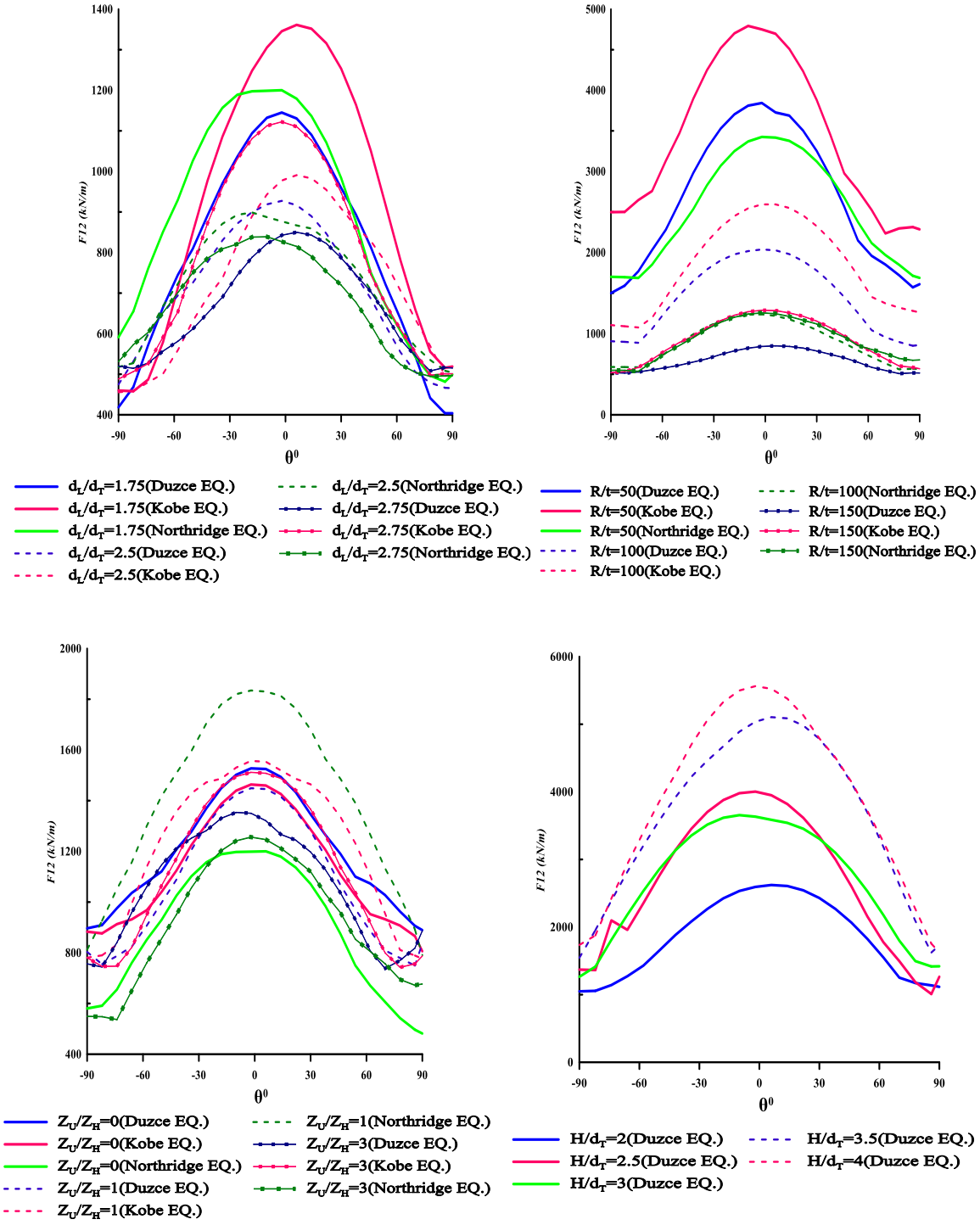

Figure B 7 Shear force for curvature, thickness, and neck level and slenderness effect respectively left to right

Appendix C

Height(m)	Analytic solution		SAP software	
	Nϕ	NΘ	Nϕ	NΘ
0	-561.38	-107.28	-560.49	-112.12
2.3203	-554.28	-105.86	-556.16	-105.87
4.64815	-547.11	-104.45	-549.16	-103.47
6.98335	-539.86	-103.04	-542.04	-102.61
9.32573	-532.52	-101.63	-534.75	-101.64
11.6751	-525.1	-100.23	-527.35	-100.34
14.0312	-517.58	-98.828	-519.86	-98.9
16.394	-509.96	-97.426	-512.27	-97.48
18.7632	-502.23	-96.022	-504.58	-96.08
21.1386	-494.38	-94.615	-496.77	-94.68
23.52	-486.41	-93.201	-488.83	-93.28
25.9073	-478.31	-91.779	-480.77	-91.87
28.3003	-470.07	-90.344	-472.56	-90.44
30.6987	-461.67	-88.894	-464.2	-89
33.1024	-453.12	-87.424	-455.68	-87.54
35.5112	-444.39	-85.928	-446.99	-86.06
37.9248	-435.48	-84.402	-438.12	-84.54
40.3432	-426.38	-82.84	-429.06	-82.99
42.766	-417.08	-81.234	-419.79	-81.4
45.1931	-407.56	-79.578	-410.31	-79.76
47.6244	-397.82	-77.863	-400.6	-78.06
50.0596	-387.84	-76.081	-390.66	-76.29
52.4985	-377.61	-74.223	-380.47	-74.45
54.9409	-367.13	-72.279	-370.02	-72.52
57.3867	-356.38	-70.24	-359.31	-70.5
59.8356	-345.36	-68.096	-348.32	-68.37

62.2874	-334.06	-65.837	-337.05	-66.13
64.742	-322.47	-63.454	-325.5	-63.76
67.1991	-310.6	-60.938	-313.66	-61.26
69.6585	-298.43	-58.282	-301.52	-58.62
72.1202	-285.98	-55.479	-289.09	-55.83
74.5837	-273.23	-52.524	-276.37	-52.89
77.0491	-260.2	-49.414	-263.36	-49.79
79.516	-246.9	-46.151	-250.08	-46.54
81.9842	-233.32	-42.734	-236.52	-43.08
84.4536	-219.5	-39.17	-222.71	-39.56
86.924	-205.43	-35.466	-208.65	-35.89
89.3952	-191.14	-31.632	-194.39	-32.27
91.8669	-176.65	-27.682	-179.99	-28.35
94.339	-161.98	-23.631	-165.32	-22.61
96.8112	-180.82	-16.904	-150.27	-15.16
99.2835	-162.88	-13.741	-135.39	-10.45
101.756	-144.87	-10.556	-120.48	-7.7
104.227	-126.82	-7.3574	-105.43	-5.03
106.698	-108.73	-4.1559	-90.32	-2.16
109.168	-90.608	-0.9612	-75.2	0.77
111.637	-72.474	2.21697	-60.08	3.67
114.105	-54.336	5.36977	-44.98	6.5
116.572	-36.205	8.48879	-29.94	9.26
119.037	-18.09	11.5665	-14.96	12.19
121.5	0	14.596	0	14.2